ARTICLE

doi:10.1038/nature19791

Accurate *de novo* design of hyperstable constrained peptides

Gaurav Bhardwaj[1,2]*, Vikram Khipple Mulligan[1,2]*, Christopher D. Bahl[1,2]*, Jason M. Gilmore[1,2], Peta J. Harvey[3], Olivier Cheneval[3], Garry W. Buchko[4], Surya V. S. R. K. Pulavarti[5], Quentin Kaas[3], Alexander Eletsky[5], Po-Ssu Huang[1,2], William A. Johnsen[6], Per Jr Greisen[1,2,7], Gabriel J. Rocklin[1,2], Yifan Song[1,2,8], Thomas W. Linsky[1,2], Andrew Watkins[9], Stephen A. Rettie[2], Xianzhong Xu[5], Lauren P. Carter[2], Richard Bonneau[10,11], James M. Olson[6], Evangelos Coutsias[12], Colin E. Correnti[6], Thomas Szyperski[5], David J. Craik[3] & David Baker[1,2,13]

Naturally occurring, pharmacologically active peptides constrained with covalent crosslinks generally have shapes that have evolved to fit precisely into binding pockets on their targets. Such peptides can have excellent pharmaceutical properties, combining the stability and tissue penetration of small-molecule drugs with the specificity of much larger protein therapeutics. The ability to design constrained peptides with precisely specified tertiary structures would enable the design of shape-complementary inhibitors of arbitrary targets. Here we describe the development of computational methods for accurate *de novo* design of conformationally restricted peptides, and the use of these methods to design 18–47 residue, disulfide-crosslinked peptides, a subset of which are heterochiral and/or N–C backbone-cyclized. Both genetically encodable and non-canonical peptides are exceptionally stable to thermal and chemical denaturation, and 12 experimentally determined X-ray and NMR structures are nearly identical to the computational design models. The computational design methods and stable scaffolds presented here provide the basis for development of a new generation of peptide-based drugs.

The vast majority of drugs currently approved for use in humans are either proteins or small molecules. Lying between the two in size, and integrating the advantages of both[1,2], constrained peptides are an under-explored frontier for drug discovery. Naturally occurring constrained peptides, such as conotoxins, chlorotoxin, knottins and cyclotides, play critical roles in signalling, virulence and immunity, and are among the most potent pharmacologically active compounds known[3]. These peptides are constrained by disulfide bonds or backbone cyclization to favour binding-competent conformations that precisely complement their targets. Inspired by the potency of these compounds, there have been considerable efforts to generate new bioactive molecules by re-engineering existing constrained peptides using loop grafting, sequence randomization and selection[4]. Although powerful, these approaches are hindered by the limited variety of naturally occurring constrained peptide structures and the inability to achieve global shape complementarity with targets. There is need for a method of creating constrained peptides with new structures and functions that provides precise control over the size and shape of the designed molecules. A method with sufficient generality to incorporate non-canonical backbones and unnatural amino acids would enable access to broad regions of peptide structure and function space not explored by evolution.

Although there have been recent advances in protein design methodology[5–9], the computational design of covalently constrained peptides with new structures and non-canonical backbones presents new challenges. First, both backbone generation and design validation by structure prediction require new backbone sampling methods that can handle cyclic and mixed-chirality backbones. Second, methods are needed for incorporation of multiple covalent geometric constraints without introduction of conformational strain. Third, energy evaluations must correctly model amino acid chirality.

Here we describe the development of new computational methods that meet these challenges, opening this frontier to computational design. We demonstrate the power of the methods by designing a structurally diverse array of 18–47 residue peptides spanning two broad categories: (i) genetically encodable disulfide-rich peptides, and (ii) heterochiral peptides with non-canonical sequences. Genetic encodability has the advantage of being compatible with high-throughput selection methods, such as phage, ribosome and yeast display, while incorporation of non-canonical components allows access to new types of structures, and can confer enhanced pharmacokinetic properties. To explore the folds accessible to genetically encoded constrained peptides under 50 amino acids, we selected nine topologies: HH, HHH, EHE, EEH, HEEE, EHEE, EEHE, EEEH and EEEEEE (Fig. 1; we define a 'topology' as the sequence of secondary structure elements in the folded peptide, where H denotes α-helix and E denotes β-strand). To explore the expanded design space accessible with inclusion of non-canonical amino acids and backbone cyclization, we sought to cover topologies containing two to three canonical secondary structure elements: HH, HHH, EEH, EHE, HEE and EE, along with H_LH_R, a cyclic topology with left- and right-handed helices.

All of the design calculations described in this Article were carried out with the Rosetta software suite[10] and followed the same basic approach. Large numbers of peptide backbones were stochastically generated as described in the following sections, combinatorial sequence design

[1]Department of Biochemistry, University of Washington, Seattle, Washington 98195, USA. [2]Institute for Protein Design, University of Washington, Seattle, Washington 98195, USA. [3]Institute for Molecular Bioscience, The University of Queensland, Brisbane, Queensland 4072, Australia. [4]Seattle Structural Genomics Center for Infectious Diseases, Earth and Biological Sciences Directorate, Pacific Northwest National Laboratory, Richland, Washington 99352, USA. [5]Department of Chemistry, State University of New York at Buffalo, Buffalo, New York 14260, USA. [6]Clinical Research Division, Fred Hutchinson Cancer Research Center, Seattle, Washington 98109, USA. [7]Global Research, Novo Nordisk A/S, DK-2760 Måløv, Denmark. [8]Cyrus Biotechnology, Seattle, Washington 98109, USA. [9]Department of Chemistry, New York University, New York, New York 10003, USA. [10]Department of Biology, New York University, New York, New York 10003, USA. [11]Center for Computational Biology, Simons Foundation, New York, New York 10010, USA. [12]Applied Mathematics and Statistics and Laufer Center for Physical and Quantitative Biology, Stony Brook University, Stony Brook, New York 11794, USA. [13]Howard Hughes Medical Institute, University of Washington, Seattle, Washington 98195, USA.
*These authors contributed equally to this work.

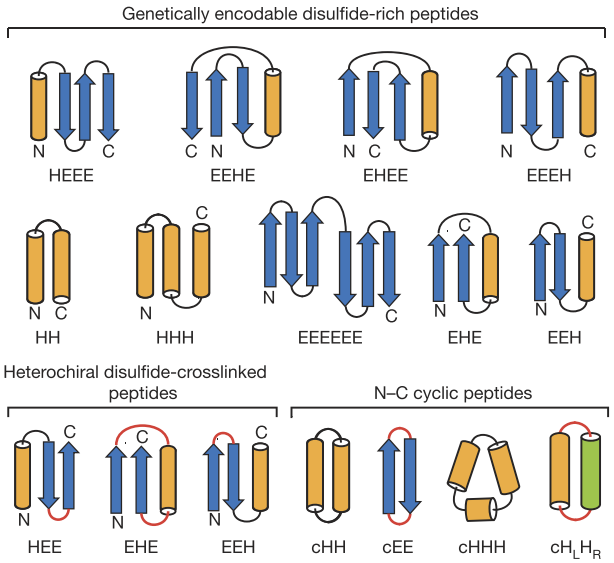

Figure 1 | Designed peptide topologies. The designed secondary structure architectures for each of the three classes of constrained peptides (genetically encodable disulfide-rich, heterochiral disulfide-crosslinked, and N–C cyclic) span most of the topologies that can be formed with four or fewer secondary structure elements. Arrows, β-strands; orange cylinders, right-handed α-helices; green cylinder, left-handed α-helix; red, loop segments containing D-amino acid residues.

calculations were carried out to identify sequences (including disulfide crosslinks) stabilizing each backbone conformation, and the designed sequence–structure pairs were assessed by determining the energy gap between the designed structure and alternative structures found in large-scale structure prediction calculations for the designed sequence. A subset of the designs in deep energy minima were then produced in the laboratory, and their stabilities and structures were determined experimentally.

Genetically encodable disulfide-constrained peptides

To design disulfide-stabilized genetically encodable peptides, we created a 'blueprint' specifying the lengths of each secondary structure element and connecting loop for each topology. Ensembles of backbone conformations were generated for each blueprint by Monte Carlo-based assembly of short protein fragments[9], or, in the case of HH and HHH topologies, by varying the parameters in backbone generating equations[11]. The backbones were scanned for sites capable of hosting disulfide bonds with near-ideal geometry, and one to three disulfide bonds were incorporated. Low-energy amino acid sequences were designed for each disulfide-crosslinked backbone using iterative rounds of Monte Carlo-based combinatorial sequence optimization while allowing the backbone and disulfide linkages to relax in the Rosetta all-atom force field (see Methods). Except for the EHEE topology, we performed no manual amino acid sequence optimization. Rosetta *ab initio* structure prediction calculations were carried out for each designed sequence, and synthetic genes were obtained for a diverse set of 130 designs for which the target structure was in a deep global free-energy minimum (Fig. 2a, b).

Disulfide bonds in peptides are unlikely to form in the reducing environment of the cytoplasm, so designs were secreted from *Escherichia coli* or cultured mammalian cells[12] (see Methods). Twenty-nine designs exhibited a redox-sensitive gel-shift, redox-sensitive high-performance liquid chromatography (HPLC) migration, and/or a circular dichroism (CD) spectrum consistent with the designed topology (see Supplementary Document 3). All 29 contain at least one non-alanine hydrophobic residue on each secondary structure element contributing van der Waals interactions in the core, which are probably important for proper peptide folding. We chose one representative design from each topology for further biochemical characterization.

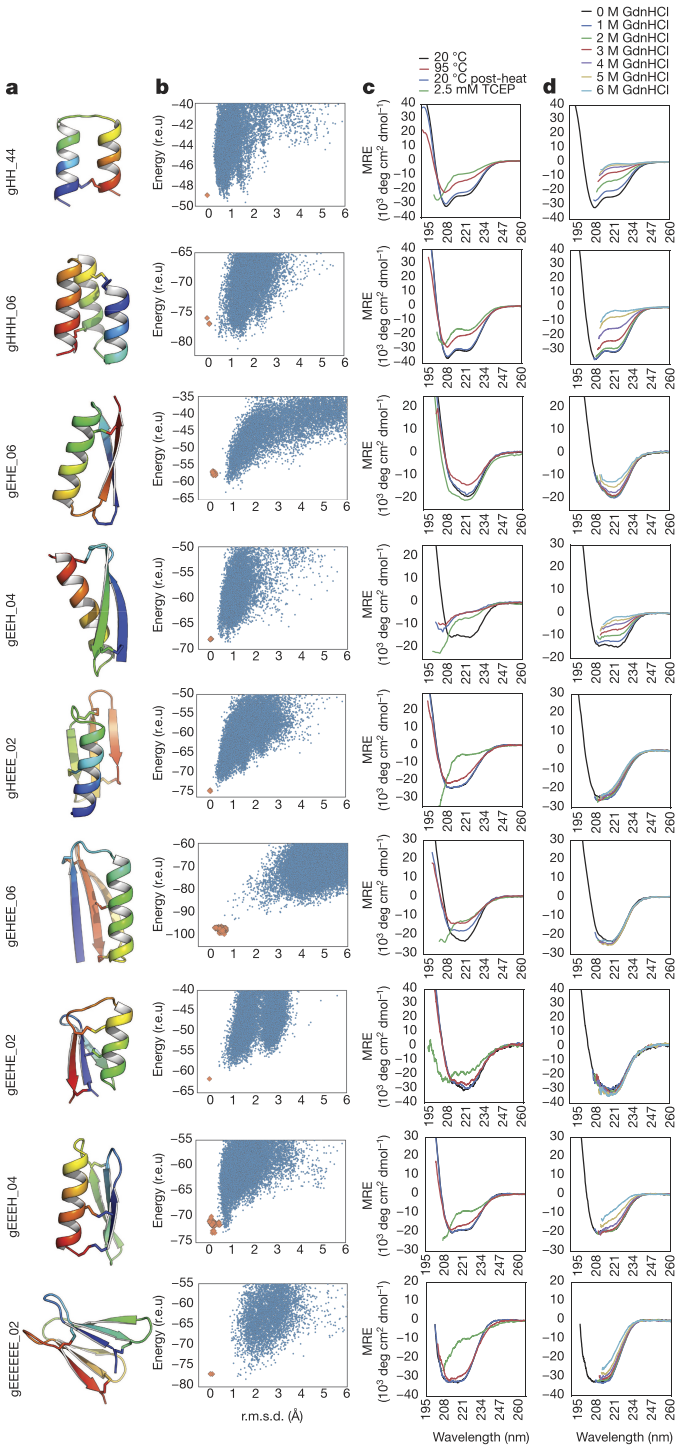

Figure 2 | Computational design and biophysical characterization of genetically encodable disulfide-rich peptides. Genetically encodable peptides are given the prefix 'g' and a number to differentiate designs that share a common topology (peptide name at far left). **a**, Cartoon renderings of each design shown with rainbow colouring from the N terminus (blue) to the C terminus (red); disulfide bonds are shown as sticks. **b**, The energy landscape of each designed sequence was assessed by Rosetta structure prediction calculations starting from an extended chain (blue dots) or from the design model (orange dots); lower energy structures were sometimes sampled in the former because disulfide constraints were only present in the latter (r.e.u., Rosetta energy units; r.m.s.d., root mean square deviation from the designed topology). **c**, CD spectra at 20 °C (black lines), after heating to 95 °C (red lines), and upon cooling back to 20 °C (blue lines). Spectra collected with 2.5 mM TCEP are shown in green (MRE, mean residue ellipticity). **d**, CD spectra as a function of GdnHCl concentration (see key).

Since eight of the nine topologies contained four or more cysteine residues, we used multiple-stage mass spectrometry to investigate the disulfide connectivity. In all cases the data were consistent with the designed connectivity (see Supplementary Document 4).

The stability of the designs to thermal and chemical denaturation was assessed by CD spectroscopy. Samples were heated to 95 °C (Fig. 2c), or incubated with increasing concentrations of guanidinium hydrochloride (GdnHCl) (Fig. 2d). The contribution of disulfide bonds to protein folding was assessed by incubating samples with a ~100-fold molar excess of the reductant tris(2-carboxyethyl)phosphine (TCEP). Designs gHEEE_02, gEEEH_04 and gEEEEEE_02 are resistant to both thermal and chemical denaturation, while design gHH_44 is resistant to thermal denaturation. gHEEE_02 contains three disulfide bonds, with each secondary structure element participating in at least one disulfide bond, and no two secondary structure elements sharing more than one disulfide bond. gEEEH_04 has two of three disulfide bonds linking the N-terminal β-strand to the C-terminal α-helix. gEEEEEE_02 consists of two antiparallel β-sheets packing against one another in a sandwich-like arrangement, with each β-sheet stabilized by a disulfide bond linking one terminus to its adjacent β-strand. gHH_44 consists of two α-helices with a single disulfide bond connecting the termini.

We crystallized design gEHEE_06 and determined the structure to a resolution of 2.09 Å (Fig. 3, Supplementary Table 2-2). The crystals had three-fold non-crystallographic symmetry, and each protomer aligns to the design model with a mean all-atom root mean square deviation (r.m.s.d.) of 1.12 Å. All three of the designed disulfide bonds were well-defined by electron density (Extended Data Fig. 1), and rotamers of core residues exhibited excellent agreement with the design model. The protein was thermostable and completely resistant to chemical denaturation (Fig. 2c, d). While gEHEE_06 shares the short-chain scorpion toxin topology, the length of secondary structure elements and loops, and the position of the disulfide bonds, are entirely divergent from known natural peptides.

As crystallization efforts for other designs were unsuccessful (with phase-separation rather than protein precipitation observed), we expressed isotope-labelled peptides in *E. coli*, and determined structures by nuclear magnetic resonance (NMR) spectroscopy[13,14] (see Methods). Upfield chemical shifts of the cysteine β-carbons[15] (deposited in the Biological Magnetic Resonance Data Bank) confirmed the formation of the designed disulfide bonds. Design gEEHE_02, with one disulfide bond connecting the termini within the β-sheet and two between the α-helix and β-sheet, aligns to the NMR ensemble with a mean all-atom r.m.s.d. of 1.44 Å. This design was impervious to both thermal and chemical denaturation (monitored by CD spectroscopy), and remained partially folded in the presence of TCEP. The final three designs are each composed of three secondary structure elements, with termini located at opposite ends of the molecule and two disulfide bonds connecting each terminus to the middle structural element or adjacent loop. gEEH_04 was less resistant than the others to thermal denaturation, but its NMR structure is nearly identical to the design model (mean all-atom r.m.s.d., 1.29 Å). gEHE_06, which contains a solvent-exposed two-strand parallel β-sheet (rare in natural protein structures[16]), aligns to the NMR ensemble with an all-atom mean r.m.s.d. of 1.95 Å; it was thermally and chemically stable based on CD measurements, and remained folded in the presence of TCEP. gHHH_06 partially unfolds upon heating to 95 °C but returns to the folded state upon cooling; the design model aligns to the NMR ensemble with a mean all-atom r.m.s.d. of 1.74 Å. Taken together, the X-ray crystallographic and NMR structures demonstrate that our computational approach enables accurate design of protein main-chain conformation, disulfide bonds and core residue rotamers.

Synthetic heterochiral disulfide-constrained peptides

We next sought to design shorter disulfide-constrained peptides incorporating both L- and D-amino acids. We generalized the Rosetta energy function to support D-amino acids by inverting the torsional potentials used for the equivalent L-amino acids (see Methods and Supplementary Information), and sequence design algorithms were extended to enable mixed-chirality design. Since chemical synthesis is labour-intensive, we prioritized the development of automated computational screening techniques, supplementing Rosetta *ab initio* screening with molecular dynamics (MD) evaluation.

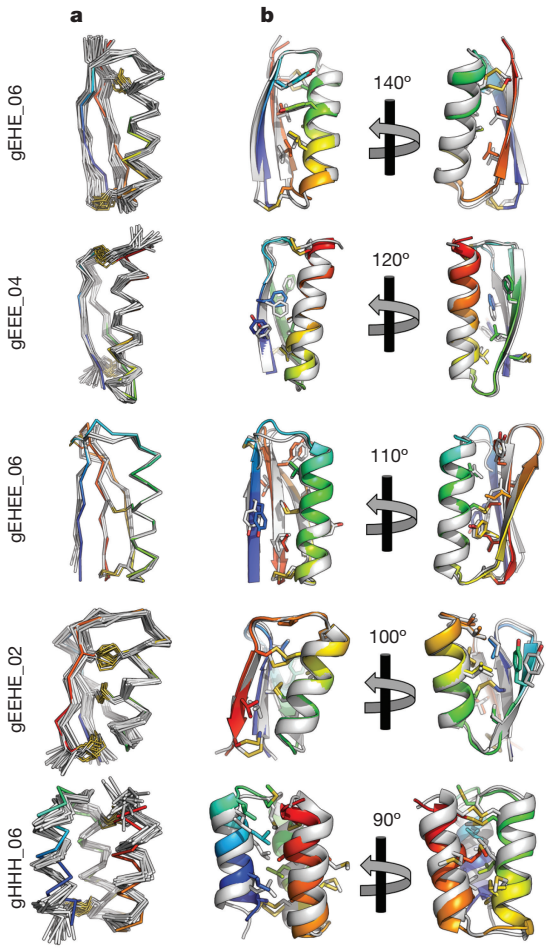

Figure 3 | X-ray crystal structures and NMR solution structures of designed peptides are very close to design models. Structures for gEHE_06, gEEH_04, gEEHE_02 and gHHH_06 were determined by NMR spectroscopy, and the structure of gEHEE_06 was determined by X-ray crystallography. **a**, C_α traces of NMR ensembles, or superimposed members of the asymmetric unit, (grey), are aligned against the design model (rainbow). Disulfide bonds are shown with sidechain atoms rendered as sticks with sulfur atoms coloured yellow. **b**, Cartoon representation of the lowest energy conformer of each NMR ensemble or crystallographic asymmetric unit (grey) is shown aligned to the design model (rainbow). Two views of each structure are shown, rotated about the vertical axis by the indicated amount. Sidechain atoms of hydrophobic core residues are rendered as sticks.

Large numbers of disulfide-constrained backbones for topologies HEE, EHE and EEH were generated by fragment assembly as described above for genetically encodable peptides. Sequences were designed (favouring D-amino acids at positions with positive mainchain ϕ dihedral angle values), and the resultant low-energy designs were evaluated using MD and *ab initio* structure prediction (Extended Data Fig. 2). For each topology, we selected a single, low-energy design (Extended Data Fig. 3) which underwent only small (<1.0 Å r.m.s.d.) fluctuations in the MD simulations (Extended Data Fig. 4) and had a large energy gap in the structure prediction calculations. Selected peptides were chemically synthesized, and structurally characterized by NMR. In all three cases, the NMR spectra had well-dispersed, sharp

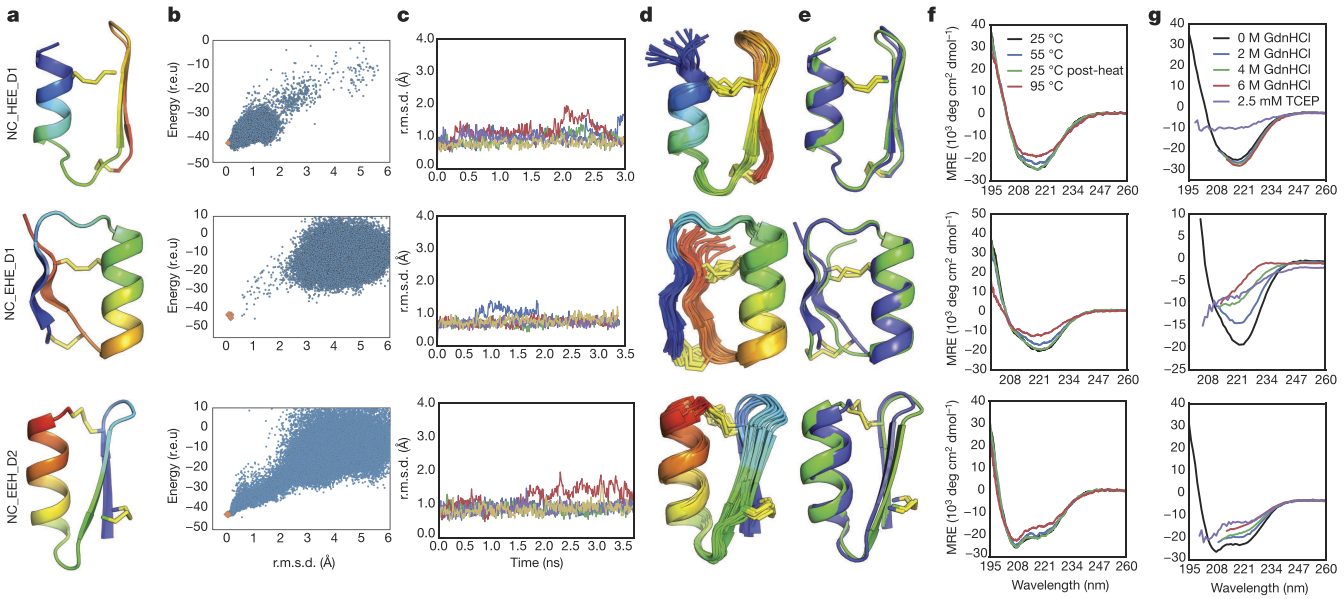

Figure 4 | Design and characterization of heterochiral disulfide-constrained peptides. The prefix 'NC' denotes non-canonical sequence or backbone architecture, and a numerical suffix differentiates designs sharing a common topology. **a**, Cartoon representations of design models with the N terminus in blue and C terminus in red. **b**, Folding energy landscapes from Rosetta *ab initio* structure prediction calculations. Blue dots indicate lowest-energy structures identified in independent Monte Carlo trajectories. Orange dots are from trajectories starting with the design model. (r.e.u., Rosetta energy units; r.m.s.d., root mean square deviation from the designed topology). **c**, Five representative trajectories from a total of 50 independent MD simulations starting from the design model with different initial velocities. **d**, NMR-determined structure ensembles. Cartoon representations coloured and oriented as in **a**. **e**, Superposition of the designed structure (blue) with the lowest-energy NMR structure (green). **f**, CD wavelength spectra between 195 nm and 260 nm recorded at 25 °C (black), 55 °C (blue), 95 °C (red) and after cooling back to 25 °C (green). **g**, CD spectra recorded at 0 M (black), 2 M (blue), 4 M (green), or 6 M GdnHCl (red), or with 2.5 mM TCEP/0 M GdnHCl (purple). Data are truncated in the far-ultraviolet region for spectra acquired in the presence of high GdnHCl concentrations (due to GdnHCl absorbance).

peaks and secondary α proton ($^1H_\alpha$) chemical shifts consistent with the secondary structure of the design model (Supplementary Fig. 2-5).

High-resolution NMR solution structures were determined for each of the designs (Supplementary Table 2-3). NC_HEE_D1 is a 27-residue peptide with a D-proline, L-proline turn at the β–β junction; in this case, Rosetta re-identified a motif known previously to stabilize type II′ turns[17,18]. The NMR structure closely matches the design model: the r.m.s.d. over all mainchain α carbon atoms (C_α r.m.s.d) is 0.99 Å between the designed structure and the lowest-energy NMR model (Fig. 4, top row). NC_EHE_D1 is a 26-residue peptide crosslinked using two disulfide bonds with a D-arginine residue in the β–α loop and a D-asparagine residue as the C-terminal capping residue for the α-helix. The design model has a 1.9 Å C_α r.m.s.d. to the lowest-energy NMR ensemble member, and a 0.68 Å C_α r.m.s.d. to the closest member of the ensemble (Fig. 4, middle row; the last two residues at the C-terminal vary considerably in the ensemble). NMR characterization of the NC_EEH_D1 design showed an unwound C-terminal α-helix adopting an extended conformation, differing from the design model (Extended Data Fig. 5). We hypothesized that substantial strain was introduced by the angle between the helix and the preceding strand, and by the disulfide bonds at both ends of the helix. A second design for the same topology, NC_EEH_D2, has a type I′ turn at the β–β connection and a different disulfide pattern. The NMR ensemble for NC_EEH_D2 is very close to the design model (0.86 Å C_α r.m.s.d. to the lowest-energy NMR model; Fig. 4, bottom row).

We explored the stability of the designed peptides using CD spectroscopy to monitor thermal and chemical denaturation. All three peptides are very thermostable; there is no loss in secondary structure for NC_HEE_D1 and NC_EEH_D2 at 95 °C, and only a small decrease for NC_EHE_D1 (Fig. 4f). Remarkably, NC_HEE_D1 does not denature in 6 M GdnHCl (Fig. 4g, top row). Treatment with TCEP causes unfolding of all three designs, highlighting the importance of disulfide bonds.

All of the designs described in this Article were created *de novo* without sequence information from natural proteins. Searches for similar sequences in the PDB and NCBI NR database using PSI-BLAST found significant alignments (*e*-value <0.01) only for NC_EHE_D1 and gHH_44 (Supplementary Table S1-2 and S1-3). The NC_EHE_D1 sequence has weak similarity (*e*-value of 2×10^{-4}) to the zinc-finger domain of lysine-specific demethylase (PDB ID: 2MA5), but the aligned regions adopt different structures (Extended Data Fig. 6). The gHH_44 sequence has weak similarity (*e*-value of 0.001) to a single long helix in a leucine zipper (PDB ID: 4R4L), very different from the helical hairpin topology of the design.

Synthetic backbone–cyclized peptides

Next, we explored the design of peptides with cyclized backbones, which can increase stability and protect against exopeptidases[19]. To generate such backbones without dependence on fragments of known structures, we implemented a generalized kinematic loop closure[20,21] method (named 'GenKIC') to sample arbitrary covalently linked atom chains capable of connecting the termini. Each GenKIC chain-closure attempt involves perturbing multiple chain degrees of freedom, then analytically solving kinematic equations to enforce loop closure with ideal peptide bond geometry in the case of N–C cyclic peptides (see Methods, Supplementary Information, and Extended Data Fig. 7). Sequence design, backbone relaxation, and *in silico* structure validation using MD simulation and Rosetta *ab initio* structure prediction were carried out with terminal bond geometry constraints (Extended Data Fig. 2).

We synthesized cyclic peptides for three topologies (cEE, cHH and cHHH) and determined their structures by NMR spectroscopy. The 18-residue NC_cEE_D1 design has the cyclic anti-parallel β-sheet fold of natural θ-defensins, but with one disulfide bond (rather than three), and different turn types containing heterochiral sequences[22]. The lowest-energy NMR model has a C_α r.m.s.d. of 1.26 Å to the designed structure. The variability in the curvature of the sheets across the NMR ensemble is similar to the variability observed in the structure prediction calculations (Fig. 5, top row). The 26-residue NC_cHH_D1

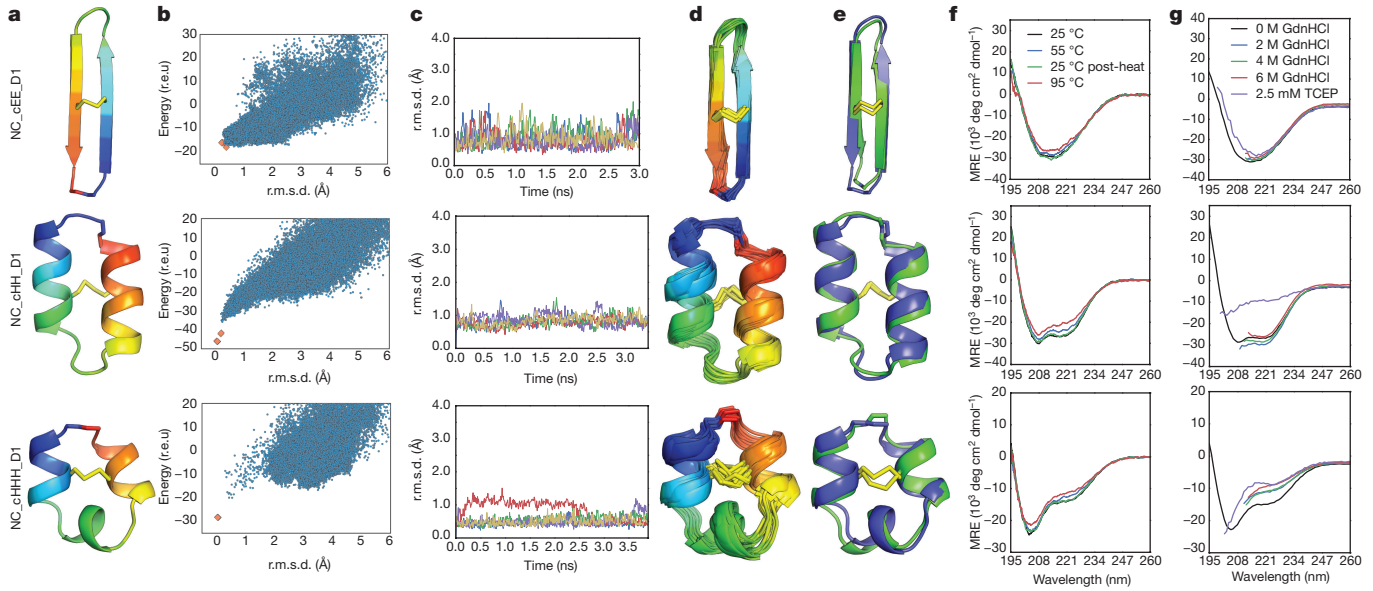

Figure 5 | Design and characterization of N-C backbone cyclic peptides. Peptide names at far left; columns **a**–**g** as in Fig. 4. A lower-case 'c' in the peptide name indicates N–C cyclic backbone.

design, which has one disulfide bond linking the two α-helices, has a 1.03 Å C_α r.m.s.d. from the lowest-energy NMR structure (Fig. 5, second row). The 22-residue NC_cHHH_D1 design has three short regions of α-helical structure and a single disulfide bond. The NMR structure of the design was again very close to the design model (Fig. 5, third row), with a C_α r.m.s.d. of 1.06 Å to the lowest-energy NMR structure.

All three cyclic topologies were found to be extremely stable in thermal denaturation experiments, retaining CD signal when heated to 95 °C (Fig. 5f). The CD spectra of NC_cHH_D1 and NC_cEE_D1 were nearly identical in 0 and 6 M GdnHCl, indicating that these peptides do not chemically denature (Fig. 5g; NC_cHHH_D1 showed some loss of secondary structure in 6 M GdnHCl). After treatment with TCEP, both NC_cHH_D1 and NC_cHHH_D1 lost secondary structure, but the CD spectrum of NC_cEE_D1 was not changed by reduction of the central disulfide bond (Fig. 5g, top row). Overall, the cyclic designs are exceptionally stable given their very small sizes.

Beyond natural secondary and tertiary structure

As a final test of the generality of the new design methodology, we designed a heterochiral, backbone-cyclized, two-helix topology with one non-canonical left-handed α-helix and one canonical right-handed α-helix (H_LH_R) assembling into a tertiary structure not observed in natural proteins. As before, we validated designs by MD; however, for validation by *ab initio* structure prediction it was necessary to develop a new, GenKIC-based structure prediction protocol (see Extended Data Fig. 8, Methods, and Supplementary Information) since the standard Rosetta *ab initio* structure prediction method utilizes fragments of native proteins, which typically do not contain left-handed helices. Our selected design for this topology, NC_H_LH_R_D1, is a 26-residue peptide with one D-cysteine, L-cysteine disulfide bond connecting the right-handed and left-handed α-helices. There is an excellent match between the NMR structure ensemble and design model (C_α r.m.s.d., 0.79 Å) (Fig. 6). As expected for the nearly achiral topology, the CD signal is very small (as observed for a previously studied two-chain, four-helix mixed D/L system[23]), and no change was observable on heating to 95 °C. The secondary $^1H_\alpha$ chemical shifts also show nearly no change on heating to 75 °C (Fig. 6g, Supplementary Fig. 2-6), indicating that the peptide is thermostable. Successful design of this topology demonstrates that our computational methods are sufficiently versatile and robust to design in a conformational space not explored by nature.

Conclusions

The key advances in computational design presented here—notably the methods for designing constrained peptide backbones spanning a broad range of topologies and incorporating natural and non-natural building-blocks—enable high-accuracy design of new peptides with exceptional thermostability and resistance to chemical denaturation. All 12 experimentally determined structures are in close agreement with the design models, including one with helices of different chirality. Unlike the natural constrained peptide families, designed peptides are not limited to particular shapes, sizes, nucleating motifs, or disulfide connectivities; indeed, the sequences of these *de novo* peptides are quite different from those of any known peptides. Here we have focused on extending sampling and scoring methods to permit design with D-amino acids and cyclic backbones, but the new tools are fully generalizable to peptides containing more exotic building-blocks, such as amino acids with non-canonical sidechains[24] or non-canonical backbones[25].

The hyperstable molecules presented in this study provide robust starting scaffolds for generating peptides that bind targets of interest using computational interface design[26] or experimental selection methods. Solvent-exposed hydrophobic residues can be introduced without impairing folding or solubility (Extended Data Figs 9 and 10, Supplementary Fig. 2-6), suggesting high mutational tolerance. Hence it should be possible to re-engineer the peptide surfaces, incorporating target-binding residues to construct binders, agonists or inhibitors. There has been considerable effort in both academia and industry to use small, naturally occurring proteins as alternatives to antibody scaffolds for library selection-based affinity reagent generation. Our genetically encoded designs offer considerable advantages as starting points for such approaches because of their high stability, small size and diverse shapes. Furthermore, having been designed exclusively to be robust and stable, they lack the often-destabilizing non-ideal structural features that arise in naturally occurring proteins from evolutionary selective pressure for a particular function. Similarly, the heterochiral designs described here provide starting points for split-pool and other selection strategies compatible with non-canonical amino acids.

Going beyond the re-engineering of our hyperstable designs to bind targets of interest, the methods developed in this Article can be used to design new backbones to fit specifically into target binding pockets. Such 'on-demand' target-specific scaffold generation is likely to yield scaffolds with considerably greater shape-complementarity than that of scaffolds generated without knowledge of the target. More generally,

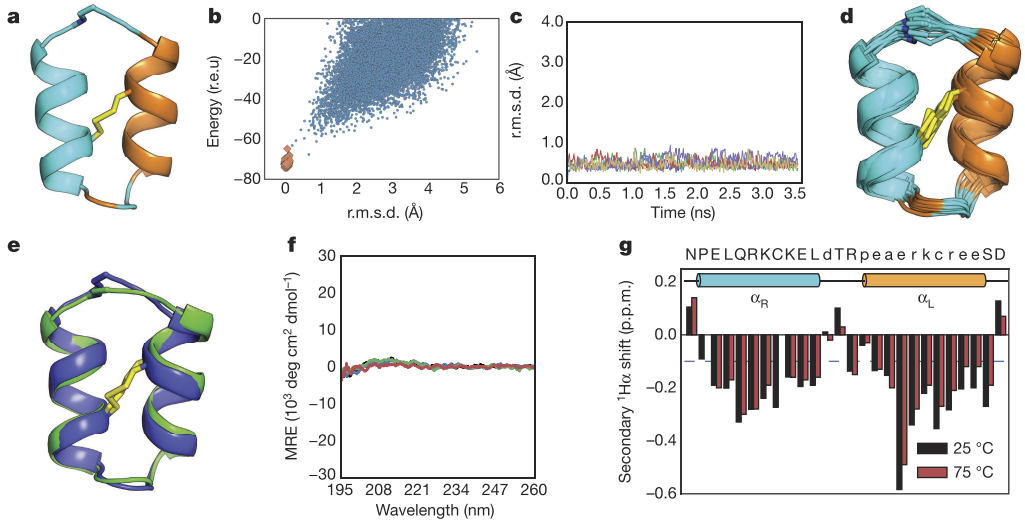

Figure 6 | Design and characterization of a peptide with non-canonical secondary and tertiary structure. a, NC_H_LH_R_D1 design (cyan, L-amino acids; orange, D-amino acids). **b**, Folding energy landscape generated using a new structure prediction algorithm compatible with non-canonical secondary structures (see Methods and Supplementary Information). **c**, Five representative MD trajectories (from a total of 50) starting from the design model with different initial velocities. **d**, NMR-determined structure ensembles, coloured and oriented as in **a**. **e**, Superposition of designed structure (blue) with lowest-energy NMR structure (green). **f**, CD spectra between 195 nm and 260 nm recorded at 25 °C (black), 55 °C (blue), 95 °C (red) and after cooling back to 25 °C (green). The CD spectrum of NC_H_LH_R_D1 exhibits very weak signals because the L- and D- helical signals largely cancel. **g**, Secondary $^1H_\alpha$ chemical shifts (p.p.m.) are nearly identical from 25 °C (black) to 75 °C (red). NC_H_LH_R_D1 sequence displayed on top; orange cylinder, left-handed helix; cyan cylinder, right-handed helix; blue dashed line represents 0.1 p.p.m. of secondary $^1H_\alpha$ chemical shifts (groups of residues with secondary $^1H_\alpha$ shifts <-0.1 p.p.m. are typically indicative of helical regions).

our computational methods open up previously inaccessible regions of shape space, and, in combination with computational interface design, should help unlock the pharmacological potential of peptide-based therapeutics.

Online Content Methods, along with any additional Extended Data display items and Source Data, are available in the online version of the paper; references unique to these sections appear only in the online paper.

Received 26 April; accepted 18 August 2016.
Published online 14 September 2016.

1. Conibear, A. C. *et al.* Approaches to the stabilization of bioactive epitopes by grafting and peptide cyclization. *Biopolymers* **106,** 89–100 (2016).
2. Craik, D. J., Fairlie, D. P., Liras, S. & Price, D. The future of peptide-based drugs.*Chem. Biol. Drug Des.* **81,** 136–147 (2013).
3. Góngora-Benítez, M., Tulla-Puche, J. & Albericio, F. Multifaceted roles of disulfide bonds. Peptides as therapeutics. *Chem. Rev.* **114,** 901–926 (2014).
4. Kimura, R. H., Levin, A. M., Cochran, F. V. & Cochran, J. R. Engineered cystine knot peptides that bind $\alpha_v\beta_3$, $\alpha_v\beta_5$, and $\alpha_5\beta_1$ integrins with low-nanomolar affinity. *Proteins* **77,** 359–369 (2009).
5. Boyken, S. E. *et al.* De novo design of protein homo-oligomers with modular hydrogen-bond network-mediated specificity. *Science* **352,** 680–687 (2016).
6. Brunette, T. J. *et al.* Exploring the repeat protein universe through computational protein design. *Nature* **528,** 580–584 (2015).
7. Lin, Y.-R. *et al.* Control over overall shape and size in de novo designed proteins. *Proc. Natl Acad. Sci. USA* **112,** E5478–E5485 (2015).
8. Doyle, L. *et al.* Rational design of α-helical tandem repeat proteins with closed architectures. *Nature* **528,** 585–588 (2015).
9. Koga, N. *et al.* Principles for designing ideal protein structures. *Nature* **491,** 222–227 (2012).
10. Leaver-Fay, A. *et al.* ROSETTA3: an object-oriented software suite for the simulation and design of macromolecules. *Methods Enzymol.* **487,** 545–574 (2011).
11. Huang, P.-S. *et al.* High thermodynamic stability of parametrically designed helical bundles. *Science* **346,** 481–485 (2014).
12. Bandaranayake, A. D. *et al.* Daedalus: a robust, turnkey platform for rapid production of decigram quantities of active recombinant proteins in human cell lines using novel lentiviral vectors. *Nucleic Acids Res.* **39,** e143 (2011).
13. Sagaram, U. S. *et al.* Structural and functional studies of a phosphatidic acid-binding antifungal plant defensin MtDef4: identification of an RGFRRR motif governing fungal cell entry. *PLoS One* **8,** e82485 (2013).
14. Liu, G. *et al.* NMR data collection and analysis protocol for high-throughput protein structure determination. *Proc. Natl Acad. Sci. USA* **102,** 10487–10492 (2005).
15. Sharma, D. & Rajarathnam, K. ^{13}C NMR chemical shifts can predict disulfide bond formation. *J. Biomol. NMR* **18,** 165–171 (2000).
16. Richardson, J. S. β-Sheet topology and the relatedness of proteins. *Nature* **268,** 495–500 (1977).
17. Syud, F. A., Stanger, H. E. & Gellman, S. H. Interstrand side chain–side chain interactions in a designed β-hairpin: significance of both lateral and diagonal pairings. *J. Am. Chem. Soc.* **123,** 8667–8677 (2001).
18. Lai, J. R., Huck, B. R., Weisblum, B. & Gellman, S. H. Design of non-cysteine-containing antimicrobial β-hairpins: structure-activity relationship studies with linear protegrin-1 analogues. *Biochemistry* **41,** 12835–12842 (2002).
19. Wang, J., Yadav, V., Smart, A. L., Tajiri, S. & Basit, A. W. Toward oral delivery of biopharmaceuticals: an assessment of the gastrointestinal stability of 17 peptide drugs. *Mol. Pharm.* **12,** 966–973 (2015).
20. Coutsias, E. A., Seok, C., Jacobson, M. P. & Dill, K. A. A kinematic view of loop closure. *J. Comput. Chem.* **25,** 510–528 (2004).
21. Mandell, D. J., Coutsias, E. A. & Kortemme, T. Sub-angstrom accuracy in protein loop reconstruction by robotics-inspired conformational sampling. *Nat. Methods* **6,** 551–552 (2009).
22. Trabi, M., Schirra, H. J. & Craik, D. J. Three-dimensional structure of RTD-1, a cyclic antimicrobial defensin from Rhesus macaque leukocytes. *Biochemistry* **40,** 4211–4221 (2001).
23. Sia, S. K. & Kim, P. S. A designed protein with packing between left-handed and right-handed helices. *Biochemistry* **40,** 8981–8989 (2001).
24. Renfrew, P. D., Douglas Renfrew, P., Choi, E. J., Richard, B. & Brian, K. Incorporation of noncanonical amino acids into Rosetta and use in computational protein-peptide interface design. *PLoS One* **7,** e32637 (2012).
25. Drew, K. *et al.* Adding diverse noncanonical backbones to Rosetta: enabling peptidomimetic design. *PLoS One* **8,** e67051 (2013).
26. Fleishman, S. J. *et al.* Computational design of proteins targeting the conserved stem region of influenza hemagglutinin. *Science* **332,** 816–821 (2011).

Supplementary Information is available in the online version of the paper.

Acknowledgements Computer time was awarded by the Innovative and Novel Computational Impact on Theory and Experiment (INCITE) program. This research used resources of the Argonne Leadership Computing Facility, a Department of Energy (DOE) Office of Science User Facility supported under contract DE-AC02-06CH11357. We thank the University of Washington Hyak supercomputing network for computing and data storage resources, and Rosetta@Home volunteer participants on BOINC for additional computing resources. We are grateful for facility access at the Queensland NMR Network. We thank D. Alonso, J. Bardwell, G. Bhabha, T.J. Brunette, D. Ekiert, A. Ford, N. Hasle, B. Keir, N. Koga, Y. Liu, D. Madden, B. Mao, D. May, V. Ovchinnikov,

S. Srivatsan, L. Stewart, R. van Deursen, and M. Williamson for help and advice, and R. Krishnamurty, P. Hosseinzadeh, and A. Vorobieva for critical comments and manuscript suggestions. This work was supported by NIH grant P50 AG005136 supporting the Alzheimer's Disease Research Center, philanthropic gifts from the Three Dreamers and Washington Research Foundation, and funding from the Howard Hughes Medical Institute. The Australian Research Council funds D.J.C. as an Australian Laureate Fellow (FL150100146). C.D.B. was supported by NIH grant T32-H600035. T.S. acknowledges NIH support (GM094597), and S.V.S.R.K.P., A.E. and X.X. were supported with NESG funds. E.C. is funded by NIGMS GM090205. We thank P. Rupert and R.K. Strong at the Fred Hutchinson Cancer Research Center for aid in collecting and refining X-ray data for gEHEE_06. G.W.B. was funded by the National Institute of Allergy and Infectious Diseases, National Institute of Health, Department of Health and Human Services (Federal contract HHSN272201200025C). A portion of this research was performed using EMSL, a DOE Office of Science User Facility sponsored by the Office of Biological and Environmental Research and located at Pacific Northwest National Laboratory.

Author Contributions C.D.B., G.B., V.K.M. and D.B. designed the study. V.K.M. developed algorithms with help from A.W., E.C., Y.S., G.B., R.B., C.D.B., G.J.R. and T.W.L. C.D.B. and J.M.G. designed canonical peptides with help from D.B., G.J.R. and T.W.L. G.B. designed heterochiral and backbone-cyclized peptides with help from V.K.M., D.B., P.G. and P.S.H. C.D.B. expressed and characterized designed canonical peptides from *E. coli* with help from J.M.G. and S.A.R. J.M.G. performed MS analysis. W.A.G. and C.E.C. purified canonical peptides *via* Daedalus and determined X-ray crystal structures. G.W.B., S.V.S.R.K.P., A.E. and T.S. determined NMR solution structures of canonical peptides, purified with isotopic labelling by C.D.B. O.C. and G.B. synthesized, purified and characterized designed non-canonical peptides. P.J.H. and D.J.C. determined NMR solution structures of non-canonical peptides. P.J.H., Q.K. and D.J.C. analysed data from structure determination of non-canonical peptides. C.D.B., G.B., V.K.M. and D.B. wrote the manuscript with help from all authors.

Author Information Peptide structures have been deposited in the RCSB Protein Data Bank with accession codes 5JG9, 2ND2, 2ND3, 5JHI, 5JI4, 5KVN, 5KWO, 5KWP, 5KWX, 5KX2, 5KWZ, 5KX1, 5KX0. Reprints and permissions information is available at www.nature.com/reprints. The authors declare no competing financial interests. Readers are welcome to comment on the online version of the paper. Correspondence and requests for materials should be addressed to D.B. (dabaker@uw.edu).

Reviewer Information *Nature* thanks V. Nanda and the other anonymous reviewer(s) for their contribution to the peer review of this work.

METHODS

Computational design. *De novo* design of constrained peptides can be divided into two main steps: backbone assembly and sequence design. Practically, our peptide design pipeline has been optimized to permit these two steps to be performed in immediate succession with a single set of inputs, with no need for export or manual curation of the generated backbones before the sequence design. (A third and final validation step is typically performed separately.)

For backbone assembly, we used two different approaches: disulfide-constrained topologies were sampled using a fragment assembly method, whereas backbone-cyclized peptide topologies were sampled using a fragment-independent kinematic closure-driven approach. Example scripts and command lines for each step in the design workflow are available in Supplementary Information.

Backbone design using fragment assembly. In the case of disulfide-crosslinked designs, the topology was defined using a 'blueprint' that specifies secondary structure and torsion bins for each amino acid residue, the latter defined using the ABEGO alphabet system[7,9]. The ABEGO nomenclature assigns a letter to each of five regions, or bins, in Ramachandran space. These bins correspond to the α-helical region (A), the β-sheet region (B), the region with positive mainchain ϕ dihedral angle values typically accessed by glycine (G), and the remainder of the Ramachandran space (E). (The fifth bin, O, represents residues with *cis*-peptide bonds, and was not used here.) The blueprint is the input for a Rosetta Monte Carlo-based fragment assembly protocol[7,9,10,27] that generates backbone conformations that match the blueprint architecture. Briefly, the fragment assembly protocol uses the defined blueprint to pick backbone fragments from a database of non-redundant high-resolution crystal structures. The insertion of fragments serves as the moves in a Monte Carlo search of backbone conformation space. For searches of the NC_EEH topology, loop types were limited to ABEGO bins EA and GG for the $\beta\beta$ connection, and BAB and GBB for the $\alpha\beta$ connection. For sampling of the NC_EHE topology, $\beta\alpha$ connections were limited to GBB, BAB and AB, and $\alpha\beta$ connections were limited to GB, GBA and AGB. For sampling of the NC_HEE topology, $\alpha\beta$ connections were limited to BAAB, GB, GBA and AGB, and $\beta\beta$ connections were limited to EA and GG.

Backbone design using generalized kinematic closure. Although the fragment-based approaches described above are powerful, they are limited to conformations that are favoured by peptides composed primarily of L-amino acids. For N–C cyclic designs—NC_cHHH_D1, NC_cHH_D1, NC_cEE_D1 and NC_cH$_L$H$_R$_D1—we chose to focus on fragment-independent methods that are better suited for exploring conformations that are accessible to only mixed D/L peptides. We therefore turned to generalized kinematic closure (GenKIC).

GenKIC-based sampling works by treating a peptide as a loop, or a series of loops to be 'closed'. The torsion values of an initial, 'anchor' residue are randomly selected; this residue is then fixed, and the rest of the peptide is treated as a loop-closure problem. The particular covalent linkages serve as a set of geometric constraints for loop closure. The GenKIC algorithm performs a series of user-controlled perturbations to the torsion angles of the peptide chain, which inevitably disrupt the geometry of the closure points. GenKIC then mathematically solves for the value of six 'pivot' torsion angles that restore the geometry of the closure points and permit the loop to remain closed[20,21,28]. Because the algorithm can return up to sixteen solutions per closure attempt, filters are applied to eliminate solutions with pivot amino acid residues in energetically unfavourable regions of Ramachandran space or with other geometric problems, such as clashes with other residues. The 'best' solution is then chosen on the basis of the Rosetta score function[10].

During the sampling steps, regions in the designed topology that were intended to form helices or sheets were initialized to ideal mainchain ϕ and ψ dihedral values, and were either kept fixed or perturbed by only small amounts ($<20°$). In loop regions, the perturbation was carried out by drawing torsion values randomly, biased by the Ramachandran preferences of the amino acid residue. Glycine or D/L alanine were used for backbone sampling before design. The allowed range of the torsion value either covered the entire Ramachandran space or, in cases in which known loop ABEGO patterns could connect secondary structure elements, the mainchain torsion values were limited to those ABEGO bins. For example, during the design of the cEE topology, connection types were limited to the GG and EA torsion bins for the two-residue loops.

Disulfide positioning. To design disulfide bonds, we evaluated all of the residue pairs with C_β atoms separated by $\leq$5 Å for geometry suitable to disulfide bond formation[27], selected backbones that could harbour disulfide bonds with near-ideal geometry, and incorporated one to three disulfide bonds. To select an ideal disulfide configuration from the set of all sterically possible combinations of disulfide bonds for a given backbone, we ranked disulfide configurations according to their effect on the configurational entropy of the unfolded state. The reduction in the entropy of the unfolded state due to a set of multiple crosslinks was computed according to a random flight model using equation (6) in ref. 29, with the volume of tolerance, ΔV, equal to 29.65 Å^3 and the link length, b, equal to 3.8 Å. This method has been implemented in the Rosetta software suite as DisulfidizeMover and DisulfideEntropyFilter, both of which are accessible to the RosettaScripts scripting language.

Modifications to Rosetta to permit design of cyclic backbones and mixed D/L peptides. D-amino acid residues allow access to regions of conformational space that are normally accessed by only glycine. When placed correctly, they can provide greater rigidity than glycine, stabilizing glycine-dependent structural motifs and, thereby, the overall fold[30]. Because the Rosetta software suite has primarily been used for designing proteins consisting of the 19 canonical L-amino acids and glycine, a number of modifications were necessary to permit robust design of peptides containing mixtures of D- and L-amino acids. First, Rosetta's default scoring function (*talaris2013* at the time of the work described here) was updated to permit D-amino acids to be scored with mirror symmetry relative their L-counterparts. Terms in the score function that are based on mainchain or sidechain torsion values were modified to invert D-amino acid torsion values before applying the equivalent L-amino acid potentials. The score-function terms that are based on interatomic distances required minimal changes. To permit energy minimization, score-function derivatives were also modified to invert torsion derivative values for D-amino acids. Rosetta's rotameric search algorithm, the *packer*, was modified to use L-amino acid rotamers with sidechain χ torsion values inverted for D-amino acid rotamer packing, and to update H_α and C_β positions appropriately when inverting residue chirality. Finally, we added an option to symmetrize the energy tables for the mainchain torsion preferences of glycine, which are asymmetric by default because they are based on statistics taken from the Protein Data Bank (PDB). (Glycine, in the context of L-amino acids only, occurs disproportionately in the positive-ϕ region of Ramachandran space, but should have no asymmetric preferences in a mixed D/L context.) Details of these modifications are described in Supplementary Information.

Because Rosetta has traditionally been used to build linear polymers, a number of core Rosetta libraries had to be modified to permit N–C cyclic geometry to be sampled and scored properly. The assumption that residue i is connected to residues $i+1$ and $i-1$, which is invalid for cyclic peptides, has been removed and replaced with proper look-ups of connected residue indices. Cyclic geometry support was tested by confirming that the circular permutations of cyclic peptide models score identically.

As of 11 March 2016, the default Rosetta score function has been changed to *talaris2014*, which re-weights a number of score terms and introduces one new term[31]. The *talaris2014* score function has also been made fully compatible with D-amino acids and cyclic geometry. A newer, experimental score function, currently called *beta_nov15*, has also been made fully compatible with D-amino acids and cyclic geometry.

Sequence design and filtering. Backbone assembly using fragment assembly or GenKIC was followed by a sequence design step. Sequence design was performed using the FastDesign protocol (see Supplementary Information). This involves four rounds of alternating sidechain rotamer optimization (during which sidechain identities were permitted to change) and gradient-descent-based energy minimization. The best-scoring structure was taken from a minimum of three repeats of FastDesign (twelve rounds of rotamer optimization and minimization). Each amino acid position was sorted into a layer ('core', 'boundary' or 'surface') on the basis of burial, and the layer dictated the possible amino acid types allowed at that position; for example, hydrophobic amino acid residues were only permitted at core positions. To favour more proline residues during sequence design, the reference weight for proline in the Rosetta score function was reduced by 0.5 units. Backbones were allowed to move during the relaxation steps. For each topology, about 80,000 structures were generated, and filtered on the basis of the overall energy per residue, score terms related to backbone quality and score terms related to the disulfide geometry. In a few cases for non-canonical peptides, a conservative mutation was manually introduced into a surface-exposed repeat sequence (for example, an arginine to break a poly-lysine sequence) to facilitate unambiguous NMR assignment.

Rosetta-based computational validation. Typically, the number of designs that can be created *in silico* exceeds the number that can be produced and examined experimentally. We therefore used Rosetta to prune the list of designs, by one of two methods. For designs consisting of canonical amino acids, Rosetta's fragment-based *ab initio* algorithm[32] was used to predict the structure of a design given its amino acid sequence, and to determine whether the target structure was a unique minimum in the conformational energy landscape. Disulfide bonds were not allowed to form during these simulations; the designed disulfide bonds are intended to stabilize an already unique global energy minimum, rather than to create a global minimum that would not otherwise exist. Designs that incorporate short stretches of D-amino acids were also validated using Rosetta's fragment-based

ab initio algorithm; the amino acid sequences of designs, with all D-amino acids mutated to glycine, were provided as input, and we allowed Rosetta to generate about 30,000 predicted structures as output. Unlike the standard *ab initio* protocol, we did not use secondary structure predictions in fragment picking. Additionally, the length of small and large fragments was set to 4 and 6 amino acid residues, respectively, instead of the default 3 and 9; we found that this produced better sampling for peptides. After conformational sampling, the D-amino acid positions were changed to their original identities and rescored. A small modification to the *ab initio* algorithm permitted it to build a terminal peptide bond for the N–C cyclic designs during the full-atom refinement stages of the structure prediction. Designs that showed no sampling near the design conformation or for which the design conformation was not the unique, lowest-energy conformation were discarded.

Because fragment-based methods are poorly suited to the prediction of structures with large amounts of D-amino acid content, such as NC_c$H_L H_R$_D1, we developed a new, fragment-free algorithm to validate these topologies. This algorithm, which we call *simple_cycpep_predict*, uses the same GenKIC-based sampling approach used to build backbones for design, with additional steps of filtering solutions on the basis of disulfide geometry, optimizing sidechain rotamers and gradient-descent energy minimization. Because the search space is vast, even with the constraints imposed by the N–C cyclic geometry and the disulfide bond(s), we further biased the search by setting mainchain torsion values for residues in the middle of the helices to helical values (a Gaussian distribution centred on $\phi = -61°$, $\psi = -41°$ for the α_R helix and on $\phi = +61°$, $\psi = +41°$ for the α_L helix); this is analogous to the biased sampling obtained by fragment-based methods, in which sequences with high helix propensity are sampled primarily with helical fragments. As with *ab initio* validation, designs showing poor sampling near the design conformation or poor energy landscapes were discarded.

Molecular-dynamics-based computational validation. We carried out further molecular-dynamics-based validation of the designs for which the *ab initio* or *simple_cycpep_predict* algorithms predicted high-quality energy landscapes. Similarly to strategies described previously[33,34], we used multiple short and independent trajectories, starting with different initial velocities to analyse the conformational flexibility and kinetic stability of the designed peptides. Molecular dynamics simulations were performed in explicit solvent conditions using the AMBER12 package and Amber ff12sb force field[35]. A rectangular water box with a 10-Å buffer of TIP3P water[36] in each direction from the peptide was used for simulations. Sodium and chloride counterions were added to neutralize the system. The solvated system was minimized in two steps: solvent was first minimized for 20,000 cycles while keeping restraints on the peptide, followed by minimization of the whole system for another 20,000 cycles. At the start of simulations, the system was slowly heated from 0 K to 300 K under constant volume with positional restraints on the peptide of 10 kcal mol^{-1} $Å^{-1}$ for 0.1 ns. For each selected peptide, 50 independent simulations starting with different initial velocities were performed. Each simulation started with the energy-minimized designed model, and was carried out for approximately 3.5 ns. Periodic boundary conditions were used with a constant temperature of 300 K using the Langevin thermostat[37] and a pressure of 1 atm with isotropic molecule-based scaling. A cut-off of 10 Å was used for the Lennard–Jones potential and the Particle Mesh Ewald method[38] to calculate long-range electrostatic interactions. The SHAKE algorithm[39] was applied to all bonds involving H atoms and an integration step of 2 fs was used for the simulations with amber12 PMEMD in the NPT ensemble. At the conclusion of the simulations, all the trajectories were analysed using the Amber12 package and VMD[40]. We looked for fluctuations in root-mean-square deviation (r.m.s.d.), and for the convergence (or lack thereof) to the designed structure among all the trajectories. The distribution of r.m.s.d. values at the end of all trajectories was also analysed, although the beginning two-thirds of each trajectory were discarded as a burn-in period. Molecular dynamics analyses for three designs of the same topology are shown in Extended Data Fig. 4.

Prediction of mutational tolerance. Because the designed peptides presented here are intended to be used as starting points for designing binders to targets of therapeutic interest, we sought to examine the extent to which the designs can tolerate mutations (such as those that must be introduced to create a binding surface). Owing to the computational expense of the mutational analysis, we focused on the NC_c$H_L H_R$_D1 design, mutating each position in sequence to each of alanine, arginine, aspartate and phenylalanine, and carrying out a full structure prediction simulation for each. These mutations covered each class of mutation (elimination of the sidechain, introduction of a positive or negative charge, introduction of a bulky aromatic sidechain or introduction of a small aliphatic sidechain). Mutations preserved chirality; that is, only D-amino acid to D-amino acid or L-amino acid to L-amino acid mutations were considered. Simulation runs were carried out on the Argonne Leadership Computing Facility's Blue Gene/Q supercomputer ('Mira') using a version of the Rosetta *simple_cycpep_predict* algorithm parallelized using the Message Passing Interface (MPI). The 127 prediction runs (each for a different mutation) each required approximately 20,000 CPU hours, and each produced about 25,000 sampled, closed conformations with good disulfide geometry. For each mutation considered, 50 trajectories were also carried out in which the mainchain was perturbed slightly and relaxed. The resulting collection of samples (from structure prediction and relaxation) was then used to calculate a goodness-of-energy-funnel metric, termed P_{near}:

$$P_{near} = \frac{\sum_{i=1}^{N} \exp\left(-\frac{\text{r.m.s.d.}_i^2}{\lambda^2}\right)\exp\left(-\frac{E_i}{k_B T}\right)}{\sum_{j=1}^{N} \exp\left(-\frac{E_j}{k_B T}\right)}$$

The value of P_{near} ranges from 0 (a poor funnel with low-energy alternative conformations or poor sampling close to the design conformation) to 1 (a funnel with a unique low-energy conformation very close to the design conformation). N is the number of samples, and E_i and r.m.s.d.$_i$ represent the Rosetta score and r.m.s.d. from the design structure of the ith sample, respectively. The parameter λ controls how close a state must be to the design if it is to be considered native-like; this was set to 1 Å. Similarly, the parameter $k_B T$ (where k_B is the Boltzmann constant and T is absolute temperature) governs the extent to which the shallowness or depth of the folding funnel affects the score; this was assigned a value of 1 Rosetta energy unit. The P_{near} metric provided a basis for comparison for the mutations considered.

Code availability. All the methods described here were implemented in the Rosetta software suite (http://www.rosettacommons.org). Rosetta software is freely available to academic and non-commercial users. Commercial licenses for the suite are available via the University of Washington Technology Transfer Office. Design protocols were implemented using the RosettaScripts interface available within the Rosetta software suite. Input files and command-line arguments for each step in our peptide design pipeline are available in Supplementary Information.

Protein purification of genetically encodable disulfide-rich peptides. Genes of designed disulfide-rich peptides were cloned into the vector pCDB180 (which we have made available via Addgene) using Gibson Assembly[41]. Protein expression from *E. coli* was carried out using a large N-terminal fusion domain consisting of the native *E. coli* protein OsmY to direct periplasmic and extracellular localization[42], a deca-histidine tag for protein purification, and the SUMO protein Smt3 from *Saccharomyces cerevisiae* to chaperone folding and provide a mechanism for scarless cleavage of the fusion from the designed protein[43]. Designed proteins were expressed from BL21*(DE3) *E. coli* (Invitrogen), and expression cultures were grown overnight with incubation at 37 °C and shaking at 225 r.p.m. Following expression via Studier autoinduction[44], a periplasmic extract[45] was prepared by washing cells with 20% sucrose, 30 mM Tris-HCl pH 8.0, 1 mM EDTA pH 8.0, 1 mg ml^{-1} lysozyme. Protein was purified from the bacterial-conditioned medium and/or the periplasmic extract by immobilized metal-affinity chromatography (IMAC). During screening, fusion protein was purified from the bacterial-conditioned medium of 50 ml cultures, which typically yielded 9 ± 4 mg of protein (before removal of the fusion protein). Protein expression from mammalian cells was carried out using the Daedalus[12] system, as previously described. With both purification systems, purified fusion proteins were cleaved by site-specific proteases, SUMO protease for *E. coli* and TEV protease for Daedalus, followed by a secondary IMAC step. The final designs were purified to homogeneity by reverse-phase high-performance liquid chromatography on an Agilent 1260 HPLC equipped with a C-18 Zorbax SB-C18 4.6 mm × 150 mm column. Solvent A (water + 0.1% TFA) and solvent B (acetonitrile + 0.1% TFA) were applied using a gradient of 0%–45% solvent B ramping linearly at a rate of 1% per minute.

Synthesis and purification of non-canonical peptides. Linear and cyclic peptides were synthesized as previously described[46]. Briefly, peptides were synthesized using automated solid-phase peptide synthesis with the Fmoc (9-fluorenylmethyloxycarbonyl) strategy. Cyclic reduced peptides were obtained after cleavage of the sidechain-protected peptides from the resin, ligation of both termini and the cleavage of sidechain protecting groups. Linear reduced peptides were collected by simultaneously cleaving the sidechain-protecting groups and the resin from the peptides. All linear or cyclic reduced peptides were oxidized at room temperature in a buffer containing 0.1 M NH_4HCO_3, in which the peptide concentration was 0.25 mg ml^{-1}. After 48 h, the mixture was acidified with trifluoroacetic acid, loaded onto a semi-preparative column and purified by RP-HPLC.

Mass spectrometry. Intact samples for each genetically encodable peptide were diluted in loading buffer with 0.1% formic acid and analysed on a Thermo Scientific Orbitrap Fusion Tribrid Mass Spectrometer via data-dependent acquisition. Liquid chromatography consisted of a 60-min gradient across a 15-cm column (internal diameter of 75 μm) packed with C_{18} resin with a 3-cm kasil frit trap (internal

diameter of 150 μm) packed with C_{12} resin. For disulfide connectivity analysis, peptides were digested with sequencing-grade modified trypsin (Promega) at a 1:50 enzyme-to-substrate concentration for 1 h at 37 °C and then desalted via mixed-mode cationic exchange (MCX). Peptide samples were dried under vacuum and resuspended in 0.1% formic acid. Digested samples were analysed using data-dependent acquisition and targeted methods.

Thermal and chemical denaturation experiments. Circular dichroism (CD) wavelength and temperature scans were recorded on an AVIV model 420 or Jasco J-1500 CD spectrometer. For thermal denaturation, peptides samples were prepared at 0.07–0.2 mg ml^{-1} final concentration in 10 mM sodium phosphate buffer (pH 7.0). Wavelength scans from 195 nm to 260 nm were recorded at 25 °C, 55 °C, 95 °C and again after cooling back to 25 °C. For chemical denaturation experiments, samples for each peptide were prepared in the presence of 0–6 M GdnHCl concentrations. The concentration of GdnHCl was measured by refractometry[47]. Peptide samples were also prepared in the presence of 2.5 mM TCEP (TCEP was pre-equilibrated to pH 7.0 before addition) and incubated for 3 h. Peptide concentrations were the same across all samples. Wavelength scans from 190 nm to 260 nm were recorded for each sample in a 0.1-cm cuvette.

NMR analysis and structure determination of genetically encodable disulfide-rich peptides. Agilent NMR spectrometers operating at ^{1}H resonance frequencies between 500 MHz and 750 MHz equipped with $^{1}H\{^{15}N,^{13}C\}$ probes were used to acquire NMR data for gEHE_06, gEEHE_02, gEEH_04 and gHHH_06. The peptides were all uniformly ^{15}N-labelled. Peptide gEEH_04 was also about 10% labelled with ^{13}C. The peptides were dissolved in 50 mM sodium chloride, 20 mM sodium acetate, pH 4.8 (gEHE_06 and gEEHE_02) or 50 mM sodium phosphate, 4 μM 4,4-dimethyl-4-silapentane-1-sulfonic acid, 0.02% sodium azide, pH 6.0 (gEEH_04 and gHHH_06). Final peptide concentrations ranged from 0.5 to 1.5 mM. The ^{1}H, ^{13}C and ^{15}N chemical shifts of the backbone and sidechain resonances were assigned by analysis of 2D [^{15}N,^{1}H] HSQC, [^{13}C,^{1}H] HSQC (aliphatic and aromatic), [^{1}H,^{1}H] TOCSY and [^{1}H,^{1}H] NOESY spectra, and 3D ^{15}N-resolved [^{1}H,^{1}H] TOCSY, ^{15}N-resolved [^{1}H,^{1}H] NOESY, HNCA, HNCO and HNHA spectra acquired at 20 °C (for gEHE_06 and gEEHE_02) or 25 °C (gEEH_04 and gHHH_06). Mixing times of 90 ms (gEHE_06 and gEEHE_02) and 200 ms (gEEH_04 and gHHH_06) were used for 2D and 3D NOESY, respectively. Slowly exchanging amides were identified for gEHE_06 and gEEHE_02 by lyophilizing a ^{15}N-labelled protein, re-dissolving in D_2O, and collecting a 2D [^{15}N,^{1}H] HSQC spectrum about 10 min after re-dissolving the protein. The resulting D_2O sample was subsequently used to collect additional 2D [^{1}H,^{1}H] TOCSY and [^{1}H,^{1}H] NOESY data. Stereospecific assignments for the Val and Leu methyl groups were obtained for gEEH_04 for the 10% fractionally ^{13}C-labelled sample[48,49]. Because it was not economical to prepare uniformly ^{13}C-labelled peptides by autoinduction, established triple-resonance NMR backbone assignment protocols could not be used. Instead, the carbon resonances were assigned by analysing the 2D [^{1}H,^{1}H] TOCSY spectra along with [^{13}C,^{1}H] HSQC spectra (collected at natural ^{13}C abundance for gHHH_06, gEHE_06 and gEEHE_02). For gEEH_04, which was 10% fractionally ^{13}C-labelled, the assignments were complemented with HNCA spectra. NMR data were processed using the Felix2007 (MSI) and PROSA (v6.4) programs and were analysed using the programs Sparky (v3.115), XEASY or CARA. Proton chemical shifts were referenced to internal 2,2-dimethyl-2-silapentane-5-sulfonate (DSS), whereas ^{13}C and ^{15}N chemical shifts were referenced indirectly via gyromagnetic ratios. Chemical shifts, NOESY peak lists and time-domain NMR data were deposited in the BioMagResBank (for accession numbers see Supplementary Table 2-1).

Isotropic overall rotational correlation times of 1.3–1.6 ns were inferred from averaged backbone ^{15}N spin relaxation times (http://www.nmr2.buffalo.edu/nesg.wiki), indicating that all peptides are monomeric in solution. The ^{1}H, ^{13}C and ^{15}N chemical shift assignments and NOESY peak lists were used for iterative structure calculations using the program CYANA (v2.1 and v3.97). Chemical shifts were used to derive dihedral ϕ and ψ angle constraints using the program TALOS+[50] for residues located in well-defined regular secondary structure elements. For the final structure calculation, H-bond restraints[13] were also introduced for gEHE_06 and gEEHE_02, for slowly exchanging amide protons. The resulting ensemble of 20 CYANA conformers was refined by restrained molecular dynamics in an 'explicit water bath' using the program CNS (v1.3)[51]. Structural quality was assessed using the online Protein Structure Validation Suite (PSVS, v1.5)[52]. The structural statistics are summarized in Supplementary Table 2-1. The coordinates for the 20 conformers representing the solution structures were deposited in the PDB (for accession numbers see Supplementary Table 2-1).

NMR analysis and structure determination of non-canonical peptides. Each non-canonical peptide (1 mg) was dissolved in 500 μl of 10% D_2O/90% H_2O or 100% D_2O (about pH 4). NMR spectra were recorded at 298 K on a Bruker Avance-600 spectrometer. Two-dimensional NMR experiments included TOCSY with an 80-s MLEV-17 spin lock, NOESY (mixing time of 200 ms), ECOSY and natural-abundance ^{13}C and ^{15}N HSQC. Solvent suppression was achieved using excitation sculpting. Spectra were processed using Topspin 2.1 then analysed using CcpNmr Analysis[53]. Chemical shifts were referenced to internal DSS.

Initial structures were generated using CYANA and were based on distance restraints derived from NOESY spectra recorded in both 10% and 100% D_2O. The following restraints were also included: disulfide bonds; hydrogen bonds as indicated by slow D_2O exchange and sensitivity of amide proton chemical shift to temperature; χ_1 restraints from ECOSY and NOESY data; and backbone ϕ and ψ dihedral angles generated using the program TALOS-N[54]. The final set of structures was generated within CNS[55] using torsion angle dynamics, refinement and energy minimization in explicit solvent, and protocols as developed for the RECOORD database[56]. Final structures were assessed for stereochemical quality using MolProbity[57].

X-ray crystallography. The gEHEE_06 peptide was purified by size-exclusion chromatography on an AKTA Pure using a GE HiLoad 16/600 Superdex 75-pg column, concentrated to 50 mg ml^{-1}, and crystallized by vapour diffusion over well solutions of 100 mM citrate (pH 3.5) and 25% PEG3350. Selected crystals were transferred to a cryo-solution of 100 mM citrate (pH 3.5), 20% PEG3350 and 15% glycerol. Diffraction data were collected on a Rigaku Micromax-007HF with a Saturn944+ CCD detector, and integrated and scaled with HKL-2000. Initial phases were determined by molecular replacement using Phaser[58] as implemented in the CCP4 software suite with coordinates derived from a Rosetta model for the scaffold. Molecular replacement found two molecules per asymmetric unit. This solution was iteratively refined with the program Refmac followed by model building with COOT, yielding crystallographic R values of $R_{cryst} = 39.9\%$ and $R_{free} = 42.5\%$. On the basis of the Matthews' coefficient, the crystals should have contained three molecules per asymmetric unit to have a reasonable solvent content of 45%. At this point, positive electron density appeared that enabled manual positioning of a third molecule in the asymmetric unit and improvement of the R values to $R_{cryst} = 32.0\%$ and $R_{free} = 34.9\%$. The model was further improved by including solvent molecules and TLS refinement. The quality of the final model was assessed using ProCheck and Molprobity (overall score: 100th percentile). The final model has been deposited in the PDB with accession code 5JG9. Crystallographic statistics are reported in Supplementary Table 2-2.

Surface redesign. In an attempt to reduce solubility and enhance crystallization, we redesigned solvent-exposed residues of designs representing each major topological category (mixed α/β, all β-sheet and all α-helical). Two resurfaced variants were selected for each design, bearing between one and two solvent-exposed tyrosine residues. We then expressed and purified these resurfaced designs using Daedalus, all but one of which expressed in a soluble manner and exhibited a redox-sensitive migration time by reverse-phase HPLC. We were able to obtain diffracting protein crystals for only redesign gEEHE_2.1_02_0008, which diffracted to 2.90-Å resolution (Supplementary Table 2-2). However, Matthews calculations predicted non-crystallographic symmetry with approximately 19 copies in the asymmetric unit, and attempts to phase the crystal by molecular replacement were unsuccessful, as were attempts to reproduce the crystal outside of the initial screen.

27. Huang, P.-S. *et al.* RosettaRemodel: a generalized framework for flexible backbone protein design. *PLoS One* **6,** e24109 (2011).
28. Lee, J., Lee, D., Park, H., Coutsias, E. A. & Seok, C. Protein loop modeling by using fragment assembly and analytical loop closure. *Proteins* **78,** 3428–3436 (2010).
29. Harrison, P. M. & Sternberg, M. J. Analysis and classification of disulphide connectivity in proteins. The entropic effect of cross-linkage. *J. Mol. Biol.* **244,** 448–463 (1994).
30. Rodriguez-Granillo, A., Annavarapu, S., Zhang, L., Koder, R. L. & Nanda, V. Computational design of thermostabilizing d-amino acid substitutions. *J. Am. Chem. Soc.* **133,** 18750–18759 (2011).
31. O'Meara, M. J. *et al.* Combined covalent-electrostatic model of hydrogen bonding improves structure prediction with Rosetta. *J. Chem. Theory Comput.* **11,** 609–622 (2015).
32. Bradley, P., Misura, K. M. S. & Baker, D. Toward high-resolution *de novo* structure prediction for small proteins. *Science* **309,** 1868–1871 (2005).
33. Caves, L. S., Evanseck, J. D. & Karplus, M. Locally accessible conformations of proteins: multiple molecular dynamics simulations of crambin. *Protein Sci.* **7,** 649–666 (1998).
34. Wijma, H. J. *et al.* Computationally designed libraries for rapid enzyme stabilization. *Protein Eng. Des. Sel.* **27,** 49–58 (2014).
35. Case, D. A. *et al. AMBER 12* http://ambermd.org/doc12/Amber12.pdf (Univ. California, 2012).
36. Jorgensen, W. L. & Corky, J. Temperature dependence of TIP3P, SPC, and TIP4P water from NPT Monte Carlo simulations: seeking temperatures of maximum density. *J. Comput. Chem.* **19,** 1179–1186 (1998).
37. Loncharich, R. J., Brooks, B. R. & Pastor, R. W. Langevin dynamics of peptides: the frictional dependence of isomerization rates of N-acetylalanyl-N′ -methylamide. *Biopolymers* **32,** 523–535 (1992).

38. Darden, T., York, D. & Pedersen, L. Particle mesh Ewald: an $N \cdot \log(N)$ method for Ewald sums in large systems. *J. Chem. Phys.* **98,** 10089–10092 (1993).
39. Ryckaert, J.-P., Giovanni, C. & Berendsen, H. J. C. Numerical integration of the Cartesian equations of motion of a system with constraints: molecular dynamics of *n*-alkanes. *J. Comput. Phys.* **23,** 327–341 (1977).
40. Humphrey, W., Dalke, A. & Schulten, K. VMD: visual molecular dynamics. *J. Mol. Graph.* **14,** 33–38 (1996).
41. Gibson, D. G. *et al.* Enzymatic assembly of DNA molecules up to several hundred kilobases. *Nat. Methods* **6,** 343–345 (2009).
42. Kotzsch, A. *et al.* A secretory system for bacterial production of high-profile protein targets. *Protein Sci.* **20,** 597–609 (2011).
43. Marblestone, J. G. *et al.* Comparison of SUMO fusion technology with traditional gene fusion systems: enhanced expression and solubility with SUMO. *Protein Sci.* **15,** 182–189 (2006).
44. Studier, F. W. Protein production by auto-induction in high-density shaking cultures. *Protein Expr. Purif.* **41,** 207–234 (2005).
45. Neu, H. C. & Heppel, L. A. The release of enzymes from *Escherichia coli* by osmotic shock and during the formation of spheroplasts. *J. Biol. Chem.* **240,** 3685–3692 (1965).
46. Cheneval, O. *et al.* Fmoc-based synthesis of disulfide-rich cyclic peptides. *J. Org. Chem.* **79,** 5538–5544 (2014).
47. Pace, C. N. Determination and analysis of urea and guanidine hydrochloride denaturation curves. *Methods Enzymol.* **131,** 266–280 (1986).
48. Neri, D. *et al.* Stereospecific nuclear magnetic resonance assignments of the methyl groups of valine and leucine in the DNA-binding domain of the 434 repressor by biosynthetically directed fractional carbon-13 labeling. *Biochemistry* **28,** 7510–7516 (1989).
49. Herve du Penhoat, C. *et al.* The NMR solution structure of the 30S ribosomal protein S27e encoded in gene *RS27_ARCFU* of *Archaeoglobus fulgidis* reveals a novel protein fold. *Protein Sci.* **13,** 1407–1416 (2004).
50. Shen, Y., Delaglio, F., Cornilescu, G. & Bax, A. TALOS+: a hybrid method for predicting protein backbone torsion angles from NMR chemical shifts. *J. Biomol. NMR* **44,** 213–223 (2009).
51. Linge, J. P., Williams, M. A., Spronk, C. A. E. M., Alexandre, M. J. & Michael, N. Refinement of protein structures in explicit solvent. *Proteins Struct. Funct. Bioinf.* **50,** 496–506 (2003).
52. Bhattacharya, A., Tejero, R. & Montelione, G. T. Evaluating protein structures determined by structural genomics consortia. *Proteins* **66,** 778–795 (2007).
53. Vranken, W. F. *et al.* The CCPN data model for NMR spectroscopy: development of a software pipeline. *Proteins Struct. Funct. Bioinf.* **59,** 687–696 (2005).
54. Shen, Y. & Bax, A. Protein backbone and sidechain torsion angles predicted from NMR chemical shifts using artificial neural networks. *J. Biomol. NMR* **56,** 227–241 (2013).
55. Brunger, A. T. Version 1.2 of the Crystallography and NMR system. *Nat. Protocols* **2,** 2728–2733 (2007).
56. Nederveen, A. J. *et al.* RECOORD: a recalculated coordinate database of 500 proteins from the PDB using restraints from the BioMagResBank. *Proteins Struct. Funct. Bioinf.* **59,** 662–672 (2005).
57. Chen, V. B. *et al.* MolProbity: all-atom structure validation for macromolecular crystallography. *Acta Crystallogr. D* **66,** 12–21 (2010).
58. McCoy, A. J. *et al.* Phaser crystallographic software. *J. Appl. Cryst.* **40,** 658–674 (2007).

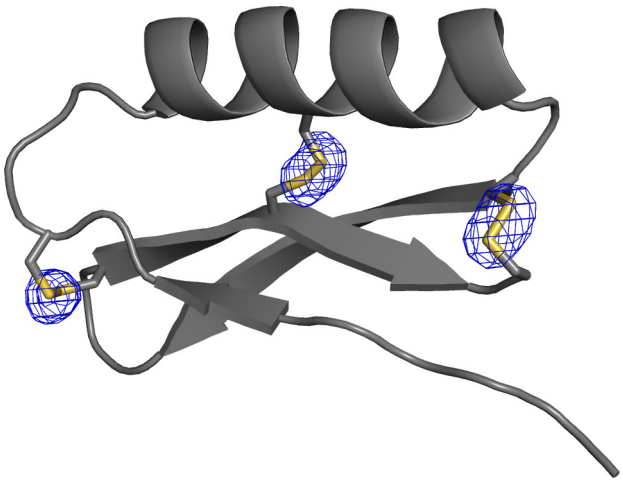

Extended Data Figure 1 | Disulfide bonds are well defined by X-ray crystallography. An $F_o - F_c$ omit-map is shown in blue, contoured at 4σ, for design gEHEE_06. Disulfide sulfur atoms were removed, and the omit-map was calculated following real-space refinement. The gEHEE_06 structure is shown in grey as a cartoon representation. Disulfide bonds are shown here as sticks, with sulfur atoms in yellow and carbon atoms in grey.

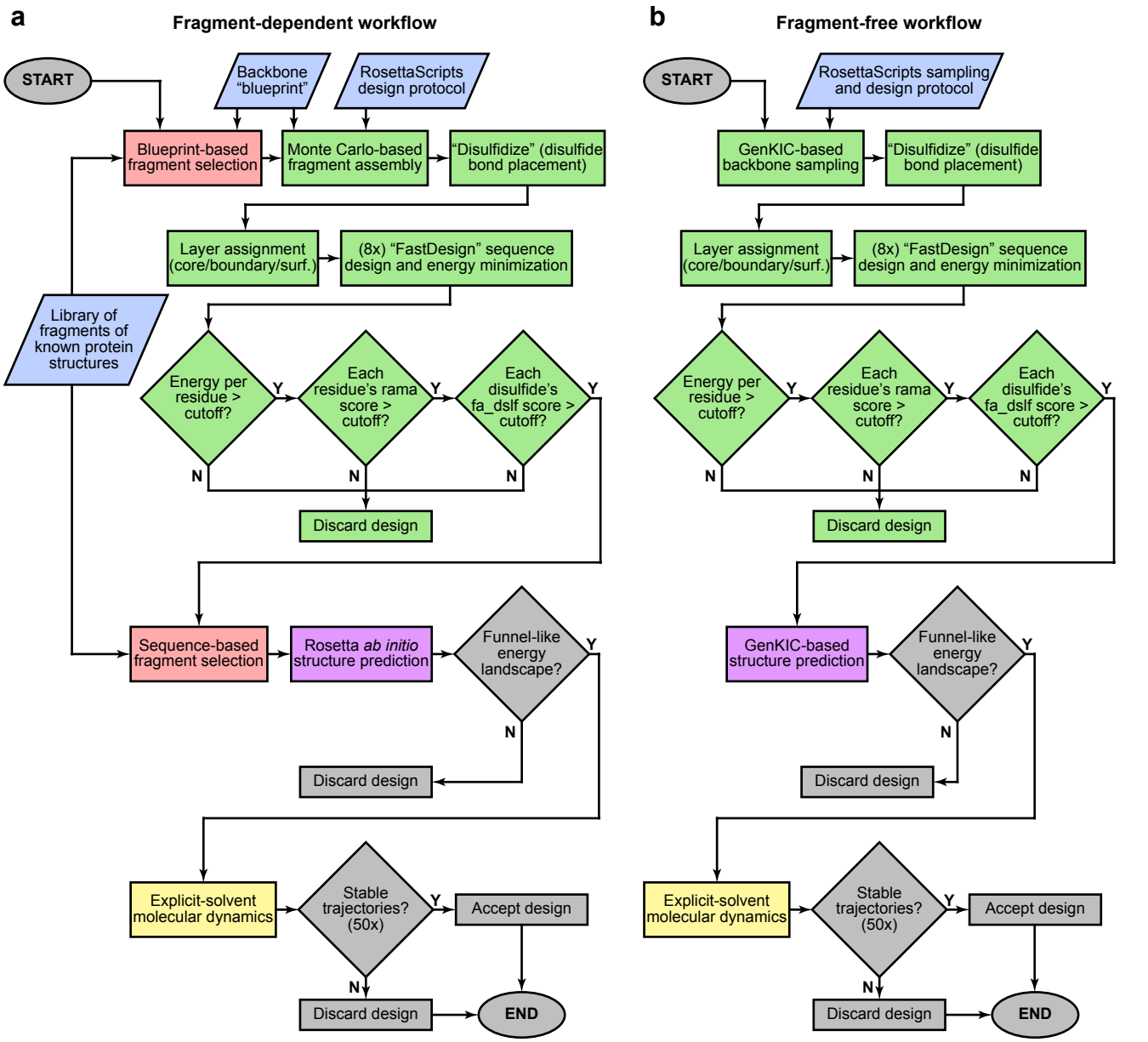

Extended Data Figure 2 | Flowchart of pipelines for designing non-canonical cyclic peptides. Inputs are shown in blue, RosettaScripts-automated parts of the pipeline are in green, parts carried out by Rosetta standalone applications are pink (the fragment picker application) and purple (the various structure prediction applications), parts performed with MD software are yellow, and manual steps are grey. **a**, Fragment-dependent design workflow. Final computational validation was carried out using MD simulations and fragment-based Rosetta *ab initio* structure prediction. For peptides containing isolated D-amino acids, these residues were mutated to glycine for Rosetta *ab initio* structure prediction. **b**, Fragment-free design workflow using GenKIC. This approach permits design of non-canonical topologies like the mixed H_LH_R topology, which occurs in no known natural protein. The GenKIC-based structure prediction algorithm is described in Extended Data Fig. 7 and in Supplementary Information.

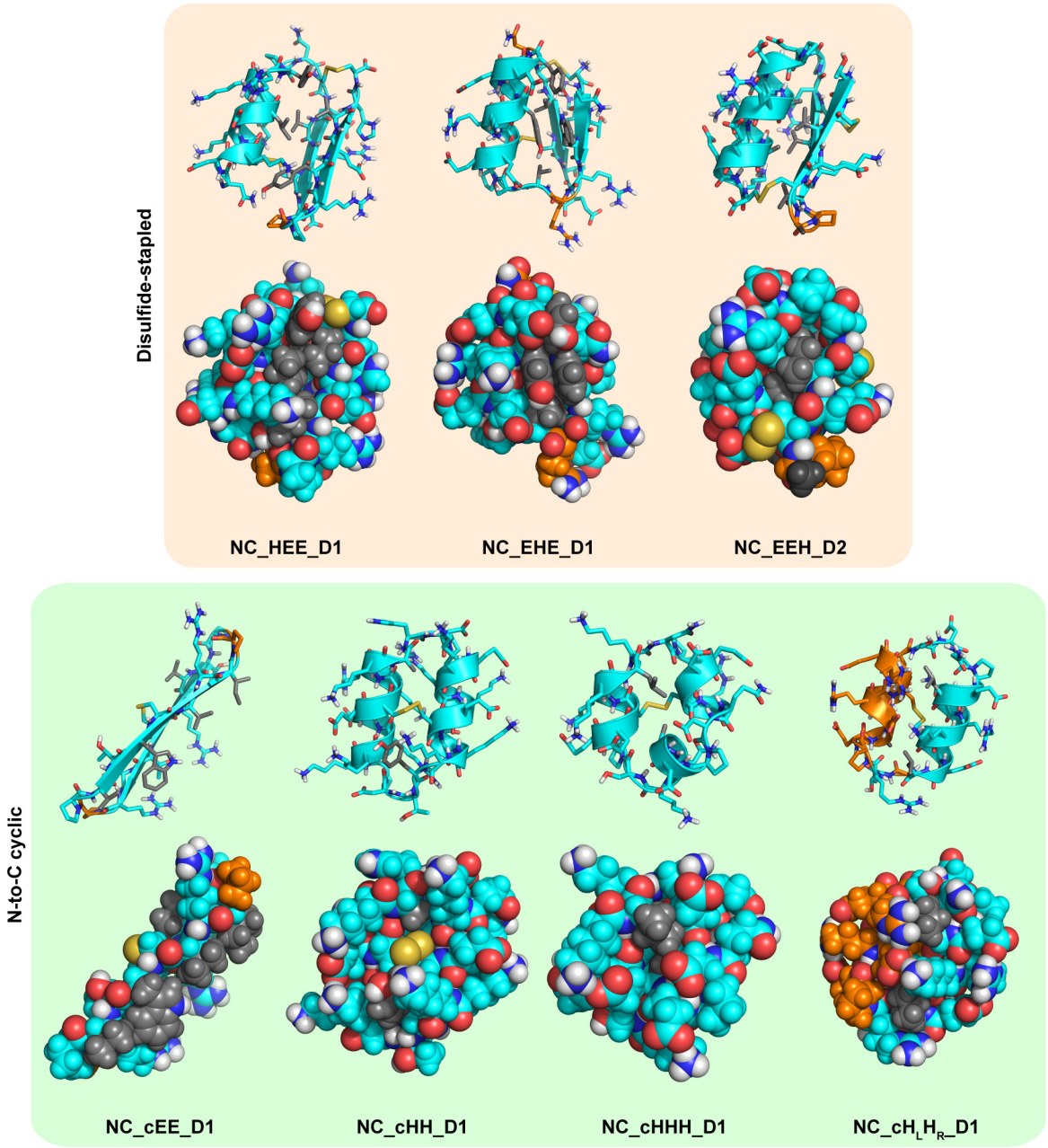

Extended Data Figure 3 | Sidechain placement in non-canonical peptide designs chosen for experimental characterization. Designs are shown as cartoon and stick representations (top row in each box) and as van der Waals spheres showing sidechain packing (bottom row in each box). L-amino acid residues are shown in cyan, and D-amino acid residues are coloured orange. Sidechains of D- or L-variants of alanine, phenylalanine, isoleucine, leucine, valine, tryptophan and tyrosine are coloured grey to aid visualization of hydrophobic packing interactions. Top box, disulfide-stapled non-canonical peptide designs; bottom box, N-to-C cyclic non-canonical peptide designs.

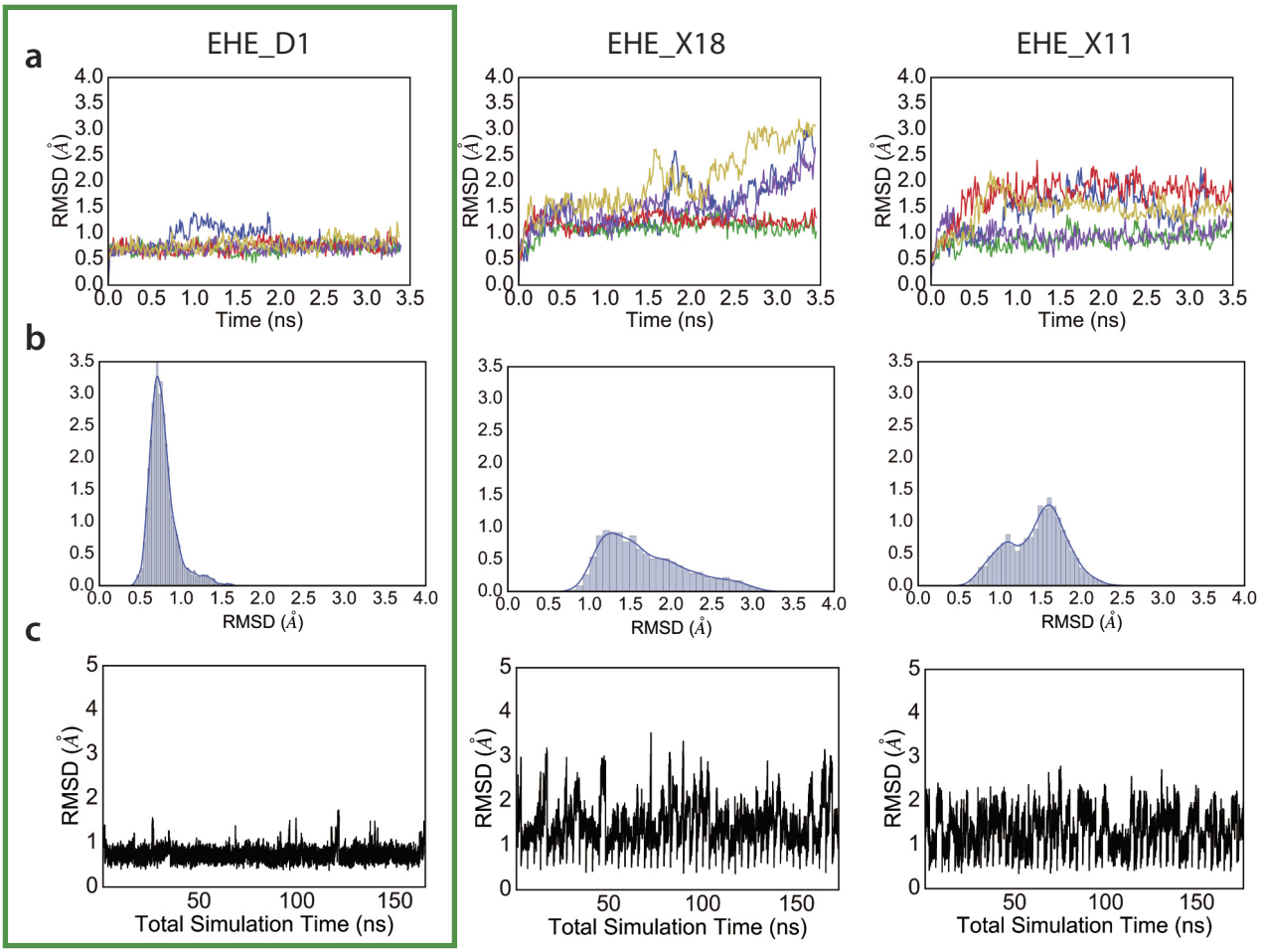

Extended Data Figure 4 | Molecular dynamics screening of designed peptides. Fifty independent molecular dynamics (MD) simulations in explicit solvent conditions, all starting from the designed peptide, were used for discriminating good, kinetically stable (for example, EHE_D1) designs from non-optimal designs of the same topology (for example, EHE_X18 and EHE_X11). **a**, Five representative trajectories from MD simulation runs. Designs that showed good convergence and smaller fluctuations were selected for further experimental characterization. **b**, r.m.s.d. distribution from all 50 trajectories. Blue line indicates the Gaussian kernel density estimate for the data. Only the last one-third of the trajectory was used for this analysis. Designs with narrower distributions were picked for further testing. **c**, Concatenated trajectory of all 50 independent runs show lower fluctuations for the more optimal designs.

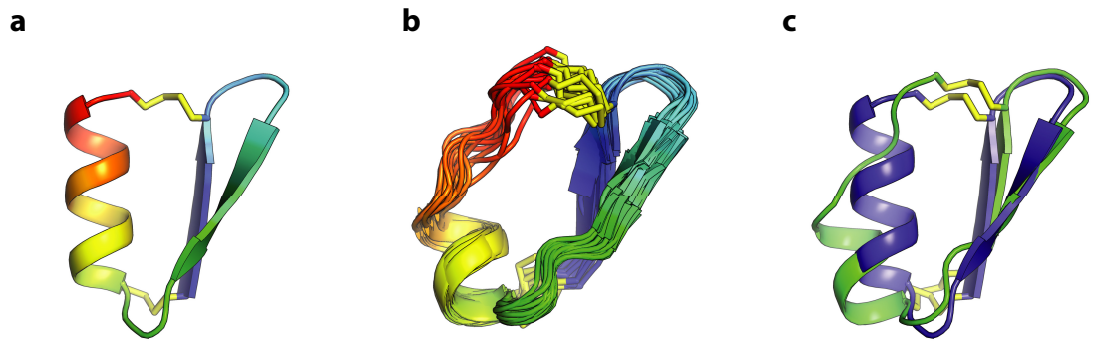

Extended Data Figure 5 | Structural characterization of NC_EEH_D1. The NMR structure of NC_EEH_D1 does not match the designed topology. **a**, Rosetta-designed model for NC_EEH_D1. **b**, Ensemble of conformers representing the NMR solution structure. **c**, Superposition of the designed model (blue) with a representative NMR conformer (green).

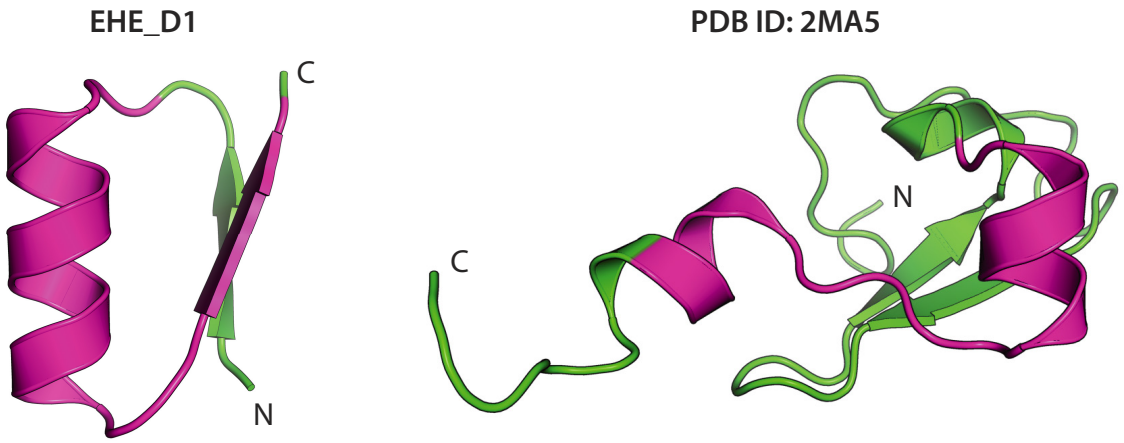

Extended Data Figure 6 | Structural mapping of sequence-aligned region between NC_EHE_D1 and 2MA5. Design NC_EHE_D1 and PDB entry 2MA5 show weak but significant (*e*-value, 2×10^{-4}) sequence alignment, which is highlighted in purple. The aligned region folds into very different structures in the different contexts of peptide and protein.

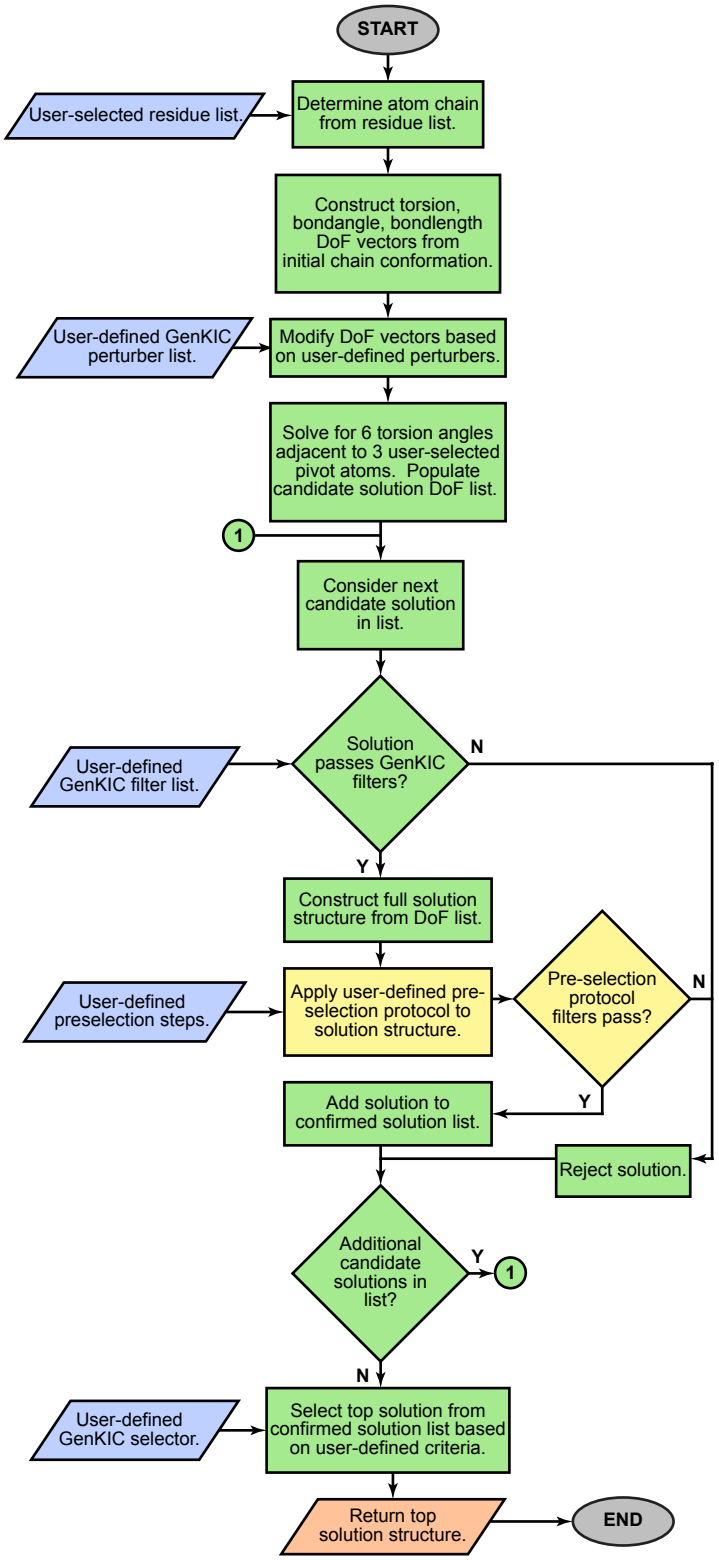

Extended Data Figure 7 | Generalized kinematic closure (GenKIC) algorithm flowchart. GenKIC allows sampling of closed conformations of arbitrary chains of atoms, passing through canonical or non-canonical backbone or sidechain linkages. Bond length, bond angle and torsional degrees of freedom in the chain can be fixed, perturbed from a starting value by small amounts, set to user-defined values, or sampled randomly. The algorithm then solves for six torsion angles adjacent to three user-defined pivot atoms in order to enforce closure of the loop. The many solutions from the closure are then filtered internally, and each can be subjected to arbitrary user-defined Rosetta protocols and filtration in order to prune the solution list further. A single solution is selected from those passing filters by a user-defined selection criterion. This flowchart shows the steps in a single invocation of the algorithm; for sampling, a user may specify that the algorithm be applied any number of times. User inputs are shown in blue, steps carried out by the GenKIC algorithm itself are in green, steps carried out by Rosetta code external to the GenKIC algorithm are shown in yellow, and outputs are shown in salmon.

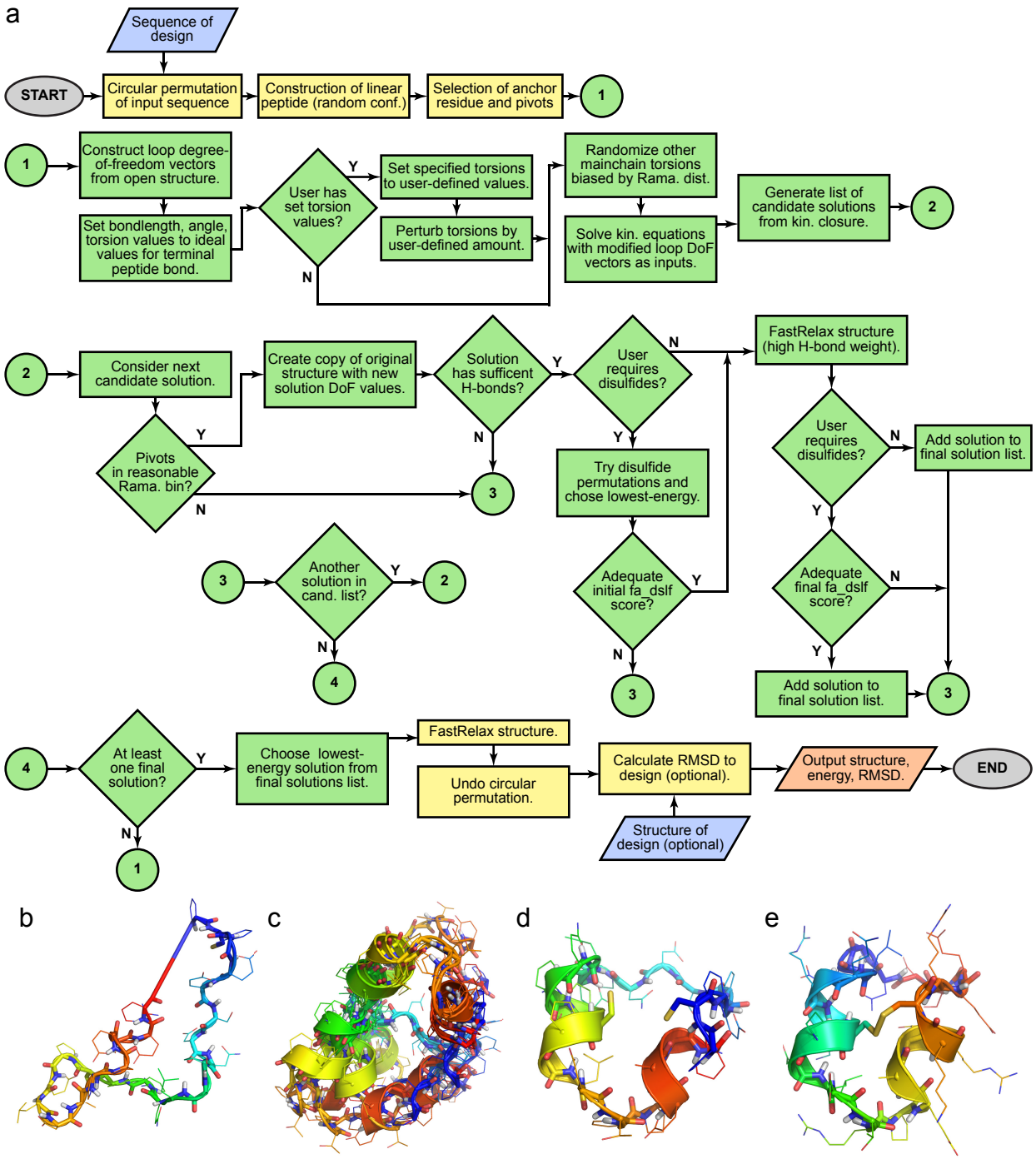

Extended Data Figure 8 | A new fragment-free structure prediction algorithm. a, Flowchart of the steps required to generate a single sampled conformation. In typical usage, this process would be repeated tens of thousands of times to produce many samples. Inputs (the peptide sequence and an optional PDB file for the design structure) are shown in blue, and outputs (the sampled structure, its energy, and its r.m.s.d. from the design structure) are shown in salmon. Steps performed by the GenKIC algorithm are shaded green, and setup and completion steps performed by the *simple_cycpep_predict* application are shown in yellow. Further details of this algorithm are discussed in Supplementary Information. **b**, The initial, random peptide conformation with bad terminal peptide bond geometry. **c**, Ensemble of closed conformations found for a single closure attempt. In this example, residue 7 (cyan) is the fixed anchor residue. Certain regions of the peptide have been set to left- or right-handed helical conformations before solving closure equations. **d**, A single closed solution with relative cysteine sidechain orientations that pass the initial, low-stringency filter for disulfide (*fa_dslf*) conformational energy. **e**, The resulting structure, following sidechain repacking, energy minimization, and cyclic de-permutation.

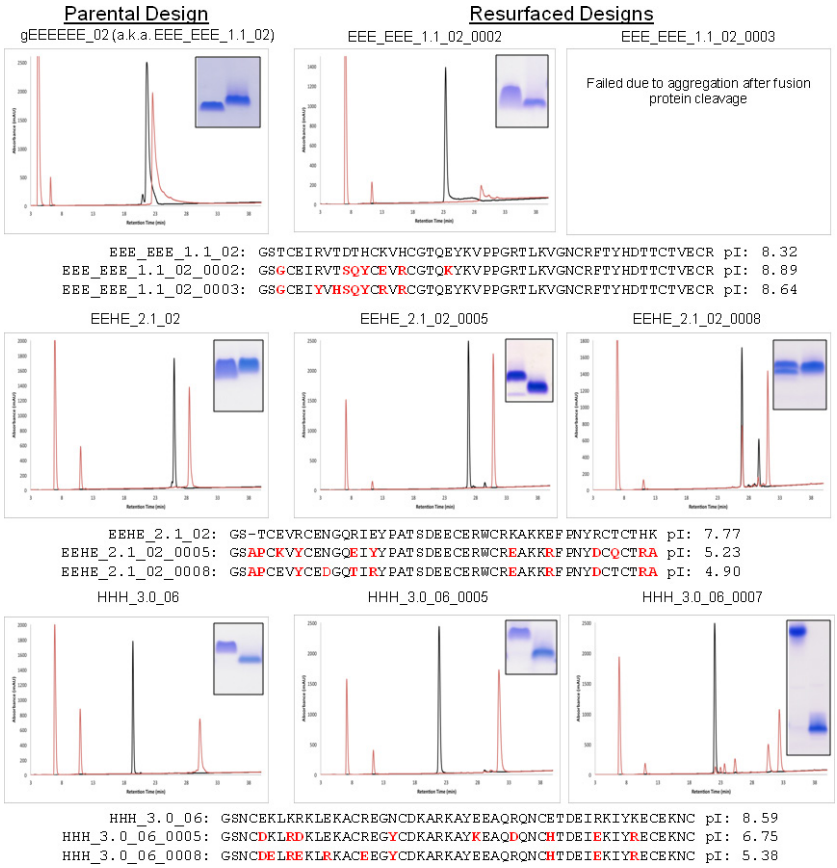

Extended Data Figure 9 | Mutational tolerance of selected genetically-encodable designs. Left column, RP-HPLC traces for the parental designs; middle and right, same for the resurfaced designs where applicable. Traces for proteins run under oxidizing conditions are shown as black lines, while traces for proteins run following reduction with 10 mM DTT are shown as red lines. Insets, gels highlighting the SDS–PAGE mobility of each purified protein under oxidizing (left band) and reducing conditions (right band). Under each row of panels are shown sequence alignments with the mutated positions highlighted in red, along with theoretical isoelectric points as calculated by ProtParam.

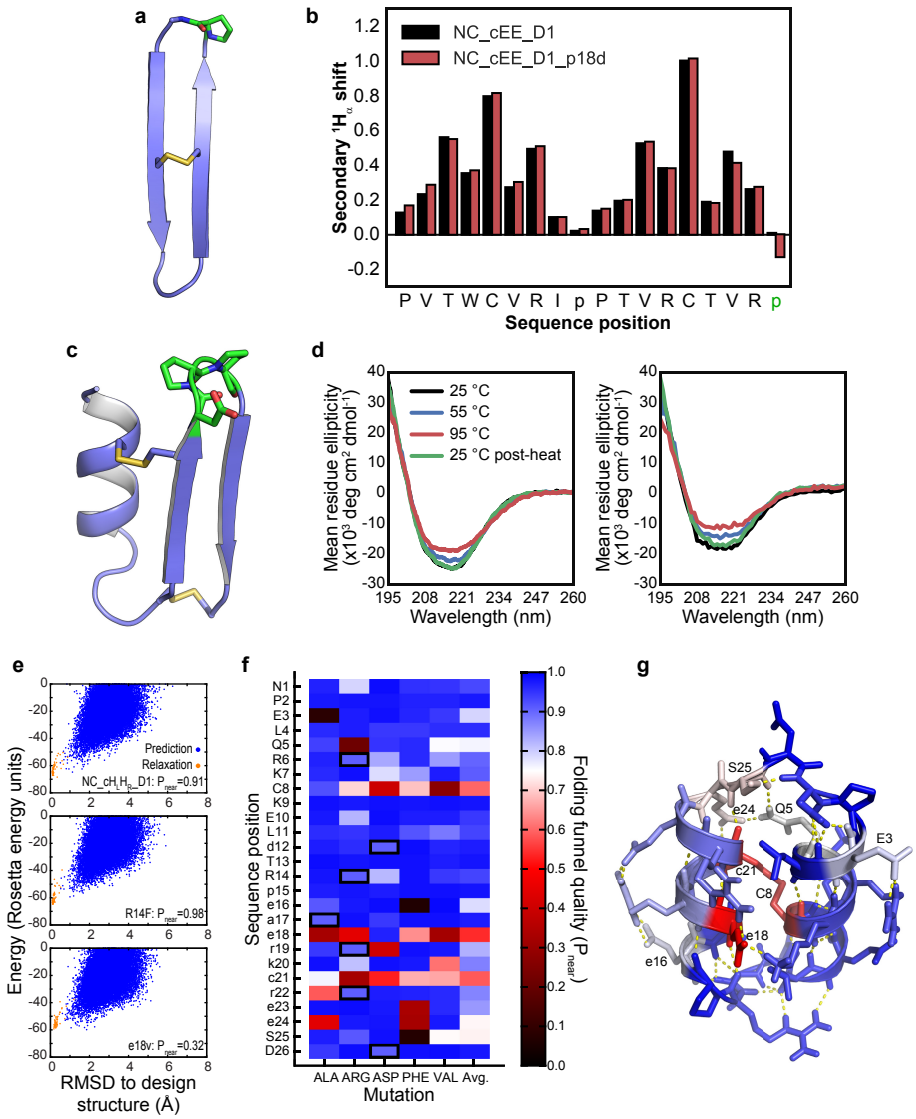

Extended Data Figure 10 | Mutational tolerance of selected NC designs. **a**, **b**, Mutational tolerance of the D-proline, L-proline loop of design NC_cEE_D1 (green in **a**), assessed by secondary $^1H_\alpha$ chemical shift (p.p.m.) for the design sequence (black bars in **b**) and the p18d loop mutation (red bars). Eliminating this key proline residue does not result in loss of β-strand signal. **c**, **d**, Mutational tolerance of loop region of design NC_HEE_D1 (green in **c**), as assessed by CD spectroscopy for the design sequence (left plot in **d**) and for the D19T, p20q, P21D triple mutant (right plot in **d**). Both proline residues may be mutated without loss of secondary structure or major change in the thermal stability. **e**–**g**, Computationally predicted mutational tolerance of design NC_H_LH_R_D1, across the entire sequence. Each position was successively mutated *in silico* to D- or L-alanine, arginine, aspartate, phenylalanine, or valine (preserving the position's chirality), and full folding simulations were carried out with the Rosetta *simple_cycpep_predict* application. Folding funnel quality was evaluated using the P_{near} metric described in Methods. **e**, Representative plots of energy versus r.m.s.d. from the design structure, plotted for the design sequence (top), for the non-disruptive R14F mutation (middle), and for the e18v mutation (bottom). Results from GenKIC-based structure prediction runs are shown in blue, and relaxation runs, in orange. Note that the bottom case shows many sampled states far from the design state with energy equal to or less than the design state energy. **f**, Mutational tolerance by position (vertical axis) and mutation (horizontal axis). Blue rectangles represent well-tolerated mutations, and red to black rectangles represent disruptive mutations, based on P_{near} evaluation of the folding funnel. Black borders indicate the design sequence. **g**, Mutational tolerance mapped onto the NC_H_LH_R_D1 structure, with colours as in **f**. Most positions tolerate mutation well, with only the disulfide bridge (C8–c21) and the salt bridges formed by e18 being highly sensitive. The hydrogen bond networks formed by residues Q5, e24 and s25 show some moderate sensitivity to mutation, as do residues E3 and e16.